Electric Power Systems Research 207 (2022) 107857

Contents lists available at ScienceDirect

Electric Power Systems Research

journal homepage: www.elsevier.com/locate/epsr

Modified methods for voltage-sag source detection using transient periods

Younes Mohammadi, Postdoctoral researcher [a,*], Roberto C. Leborgne [b], Boštjan Polajžer [c]

[a] Department of Engineering Sciences and Mathematics, Luleå University of Technology, Skellefteå campus, Forskargatan 1,93187 Skellefteå,Sweden, Tel.: +46-910-585-310

[b] Universidade Federal do Rio Grande do Sul, Osvaldo Aranha, 99, 90035-190, Porto Alegre, RS, Brazil

[c] University of Maribor, Koroška c. 46, 2000 Maribor, Slovenia

ARTICLE INFO

Keywords:
Voltage sag (dip)
Source detection
Transient period
Faster response
Modifier

ABSTRACT

Real-time detection of the voltage sag sources' relative location requires fast and accurate methods. Therefore, in this paper, the transient period of voltage sags is used with useful detection information, which is not considered in the literature. In this context, this work firstly analyses the main positive-sequence phasor-based (PB) and instantaneous-based (IB) methods within both transient and steady-state periods of voltage sags caused by network faults and transformer energizing. Secondly, new methods are proposed using five different modifiers, applied in the transient period of voltage sags, i.e., half and one cycle time windows, to achieve a faster and more accurate response. These modifiers use the PB/IB criteria obtained from the existing methods, such as power, impedance, and current, and are applied as: The mean of the criterion changes, the first largest peak (FLP) on the criterion changes, the mean of the zero-mean criteria during a sag, the FLP of the zero-mean criteria during a sag, and the Trend (slope) of criteria's trajectories versus time. Voltage sag source detection methods are evaluated by applying 1992 simulated voltage sag events in a Brazilian regional power network. The results reveal that the proposed modifiers, used in the new methods, improve the ineffective existing methods by taking half/one cycle within a transient period of voltage sags. The modifiers also show an accuracy equal to other existing enhanced methods due to employing them within the transient period, thus evidencing their appropriateness. Correspondingly, a selection is made amongst the new modified methods in order to choose the most accurate time window (half or one cycle) for the methods. The selected modified methods are also tested by applying field measurements in a Slovenian power network to confirm their effectiveness in the transient short periods. According to a recommendation of the fastest and most accurate new methods in this study, an important application can be using the recommended methods as the directional function in the relays, along with an accurate voltage sag/fault inception time detection algorithm in real-time.

1. Introduction

In the last decades, voltage sags have been considered one of the most severe events in power quality [1]. Despite their short duration, such events can cause serious problems in transmission and distribution networks, micro-grids, industrial or customer facilities. Many events, including short-circuit faults, starting/loading induction motors, and transformers' energizing, may cause voltage sags. Due to all these events (except starting the motors), the sags propagate throughout the power network, affecting connected loads far from the source location [2–4]. Therefore, monitoring, analysing, and characterizing the sag events, and also identifying their causes, can help mitigate the substantial loss of product of a typical industrial installation and improve the power quality [2]. Detecting the sag sources by a proper formulation (when there is no mitigation equipment) is an important strategy to define the responsibility of both sides of power supply and consumption for the sags caused by fault/transformer energizing in offline applications. There is a need for direction detection methods to operate as a directional function in relays and a secured backup protection to prevent the unwanted operations of protection quickly. This is where faster and more accurate methods are needed. Also, there is a lack of a comprehensive comparison of such detection methods in steady-state and transient periods of sags.

1.1. Related works

Several methods for non-real-time detecting voltage sag sources'

* Corresponding author.
E-mail addresses: Younes.mohammadi@ltu.se (Y. Mohammadi), Roberto.leborgne@ufrgs.br (R.C. Leborgne), Bostjan.polajzer@um.si (B. Polajžer).

https://doi.org/10.1016/j.epsr.2022.107857
Received 10 November 2021; Received in revised form 17 January 2022; Accepted 9 February 2022
Available online 16 February 2022

Nomenclature

CBM	Current based method
DFT	Discrete Fourier Transform
DPE	Disturbance power and energy
DR	Distance relay
DS	Downstream
E	Existing
F/Fa/Fb	Phasor-based criteria used by the modifiers
f/fa/fb	Instantaneous-based criteria used by the modifiers
FLP	First largest peak
IB	Instantaneous-based
M	Modified
PB	Phasor-based
PCSC	Phase change in sequence current
PQM	Power quality monitor
pu	Per unit values
RCC	Real current component
SM	Selected modified
SST	Slope of system trajectory
TE	Transformer energizing
US	Upstream
zm	Zero-mean
(.)	Number of the equation
$\Delta(.) = (.)_{sag} - (.)_{presag}$	Change due to sag
$\angle(.)$	Phase angle
$(.)^{+}$	Positive-sequence components
$(.)_{zm}$	Criterion by removing mean value (zero-mean)
(θ)	Phase angle between voltage and current
V, I, Z	Voltage, current and impedance phasors (line or $(.)^{+}$)
v, i, z	Instantaneous voltage, current and impedance (line or $(.)^{+}$)
P, E	Active power, and energy obtained from phasor values
p, e	Active power, and energy obtained from instantaneous values

relative location have already been reported in [5–44]. The methods for downstream (DS)-upstream (US) detection can be classified into three groups. The first and basic group consists of the analytical methods, which are based on a variety of criteria, such as disturbance power and energy [5–7], voltage-current characteristics [8, 9], change of impedance and resistance [10–14], voltage based [15–17] and current based [18–23]. Statistical methods have been applied to enhance accuracy and confidence within this group. Methods with combined rules based on stationary phasors have also been developed [24–26]. Higher effectiveness was achieved for several types of methods by applying positive-sequence phasors [27], Clark components [28–30], and instantaneous positive-sequence components [31,32]. Moreover, a short [33,34] and full [3] review has been done on some mentioned methods. A second group incorporates signal processing techniques, which develop the method presented in [5]. These methods are based on the Hilbert transform [35,36], S transform [37], and a combination of S and TT (time-time) transform [38]. A third group focuses on machine learning tools such as support vector machine and ensemble classifiers [39,40] and methods based on neural networks [41–43]. Furthermore, a data-driven approach using random matrix theory found out the location of complex sags due to multiple faults [44]. Later, a genetic algorithm was applied to select the best measurement points and locate the source of voltage sags due to faults [45].

1.2. Shortfalls of previous methods

Most of the analytical methods mentioned above have been analysed during the steady-state period of voltage sags, which was focused between three and five to six cycles after the event starting, while only a few analytical methods [8,27] are based on information available in a transient period, whereas the transient period includes source detection information due to a sudden change in the energy state of the networks.

While the short-circuit faults are the main causes of sags, transformer energizing (TE) is another important common reason for the occurred sags. The voltage sags caused by TEs differ from faults since they are always asymmetrical, have harmonic content (especially in current), and have a long recovery time between 100 and 500 ms, which can have a different impact on the loads and generators such as wind turbines [46]. The literature has shown that the existing methods focused mostly on sags due to faults, and just a few considered the sags due to a TE [27–31].

Hence, there is a lack of investigation of methods during the transient period of sags (which is considered as half and one cycle at the beginning of sags, in our study) due to both faults and TE, since extraction of some information from voltage and current signals in a transient period may enhance the performance of methods in a shorter time. Moreover, introducing methods with accurate responses within a transient period of sags can be a good candidate to be used in real-time applications. Even though there are several studies in both real and non-real-time for finding "exact" location of faults, such as [47–49], finding the "relative" location of sag sources in a short transient period after starting sags has not been studied.

On the other hand, the literature [30–32] has shown a high accuracy of the current-based methods by using instantaneous-based (IB) positive-sequence components for short duration sags and sags in networks with distributed generation and active loads (transient behaviour). Hence, it is worth checking the IB methods besides phasor-based (PB) ones within a transient period of sags.

Machine learning methods [39–45] were applied on a group of scaler features obtained from a steady-state period of sags to enhance the performances during the steady-state period. However, in real-time applications, their accuracy depends on the set of time-consuming steady-state features. Also, a critical task is to label many voltage sags recorded in the power quality monitors worldwide as an input dataset into supervised machine learning-based methods as DS/US classes. Therefore, improving the PB or IB features through introducing proper new methods during transient periods of sags, which means enhancing the accuracy of analytical methods, will make the machine learning-based methods more accurate and faster.

1.3. Contribution and applicability

The contributions of this paper are:

(a) A comprehensive analysis of the main existing methods, which use positive-sequence PB or IB values, is performed during both transient and steady-state periods of voltage sags caused by network faults and transformer energizing. The results show that some methods are more accurate when employed in transient periods, while others do not work properly under said conditions. Therefore, according to extensive simulations and field measurements for the sags with various time durations, different time windows are selected and applied, i.e., half and one cycle for a transient period, and two, three, and five (50 Hz)/six (60 Hz) cycles for the steady-state period.

(b) New methods are proposed employing five new modifiers (applied on the basis of the existing methods) during the transient period of voltage sags, which improve the ineffective existing

methods by taking half/one cycle (a shorter time) within a transient period and also show an accuracy equal to other existing methods enhanced due to employing them within the period, thus verifying their appropriateness.

These modifiers are: The mean of the criterion changes, the first largest peak (FLP) on the criterion changes, the mean of the zero-mean criteria during a sag, the FLP of the zero-mean criteria during a sag, and the Trend (slope) of criteria's trajectories versus time. The criteria are the detection rules for locating the voltage sag sources.

(a) Choosing the most accurate time window (half or one cycle) for each new method. The selected modified methods, which are the most accurate and fastest, will be endorsed, along with a fast and accurate voltage sag/fault inception time detection algorithm such as [50] as a candidate to be used in real-time. Amongst them, the methods with modifiers of Mean-zm, FLP-zm, and Trend, which don't need detection of the exact sag starting time, will be highly recommended in real-time applications.

The applicabilities of the new methods are:

(a) The applications, as real-time, include directional function in relays and a secured backup protection scheme, with high reliability, in case of faults as the source of sags. For the sags due to transformer energizing, the network operator can recognize the location of the transformer with high performance in a short time, especially the TE for which operators do not have information. An example of energizing after successful auto-reclosing protection relays was shown in [51].
(b) The planned modifiers improve single or two features required by analytical methods in the transient period. In the case of machine learning methods, which utilize (i) a set of features that is time-consuming in real-time, (ii) features are extracted from a steady-state period, which takes more time than a transient period. Therefore, the performance of the supervised and unsupervised machine learning methods can be enhanced in a shorter time by inputting a set of the improved transient features presented in this paper.

1.4. Content

The remainder of this paper is organized as follows: Section 2 presents briefly the basic methods for voltage sag source detection. Section 3 introduces the new methods. The results of existing methods and new ones on extensive simulations are explained in Section 4. Section 5 gives the results of existing and selected modified methods on field-testing. A discussion and further work are specified in Section 6, and finally, Section 7 concludes the paper.

2. Methods for voltage sag source detection

There are eight basic existing methods for voltage sag source detection, such as Disturbance Power and Energy (DPE) [5, 7], Real Current Component (RCC) [8], Slope of System Trajectory (SST) [9], Distance Relay (DR) [12,13], Current Based Method (CBM) [18,21], and Phase Change in Sequence Current (PCSC) [20], in which the direction of the sag sources concludes as DS or US relative to a Power Quality Monitor (PQM). The DS/US refers to the energy flow direction before the sag. A generalization of the basic methods of [5,7–9] was reported in [27] based on positive-sequence PB values. Another extension of methods of [5,8,9] and [18,20,21] was stated in [32] and [31], respectively, by employing positive-sequence IB values. Hence, only the extended/enhanced methods are given in Table 1 as a representative of the existing methods in the literature. Throughout this paper, symmetrical components using Fortescue transform are applied on the phasor, and instantaneous values, in which only a positive-sequence component is considered. The methods' performances for different time windows during transient and steady-state periods are investigated in Section 4.2. Results show which methods work in the transient period and which need modifications to get higher accuracy.

3. New methods for voltage sag source detection

Information on US/DS detection of voltage sag sources can be

Table 1
Description of the main existing PB and IB methods for voltage sag source detection.

Criteria	Method	Category	[Ref.]	Basic rule for DS direction (else US)	(Eq.)
Methods using changes of power: Voltage sag sources can act as energy sinks. So, the power flow at the PQMs may be increased for DS events and be decreased for US events.	E-DPE	PB	[27]	$\Delta E^{+}(t) = \int_{0}^{t} \Delta P^{+}(t)dt > 0,\ P^{+} = V^{+}I^{+}cos(\theta)^{+}$	(1.1)
		IB	[3,32]	$\Delta e^{+}(t) = \int_{0}^{t} \Delta p^{+}(t)dt > 0,\ v^{+}i^{+}cos(\theta)^{+}$	(1.2)
Methods using changes of current: Voltage sags are a result of a short-duration current increase. Thus, currents increase during DS events and decrease during US events. The criteria are based on slope of system trajectory and change in real current.	E-RCC	PB	[27]	$\Delta(I^{+}cos(\theta)^{+}) > 0$	(2.1)
		IB	[3,32]	$\int_{0}^{t} \Delta(i^{+}cos(\theta)^{+})dt > 0$	(2.2)
	E-SST	PB	[27]	slope $(I^{+}, \lvert V^{+}cos(\theta)^{+}\rvert)$ line < 0	(3.1)
		IB	[3,32]	slope $(i^{+}, \lvert v^{+}cos(\theta)^{+}\rvert)$ line < 0	(3.2)
Methods using changes of impedance: The magnitude and angle of impedance change at the PQMs during voltage sags. The criteria are based on impedance changes estimated by a distance relay.	E-DR	PB	[12, 13]	$\Delta\lvert Z^{+}\rvert(0$ and $\angle Z^{+}$ or $(\Delta\angle Z^{+}))0,\ Z^{+} = V^{+}/I^{+}$	(4.1)
		IB	[32]	$\int_{0}^{t} \Delta\lvert z^{+}\rvert dt < 0$ and $\angle z^{+}$ or $(\int_{0}^{t} \Delta\angle z^{+}dt) > 0,$ $z^{+} = v^{+}/i^{+}$	(4.2)
Methods using only current measurements: Sometimes the measurements of only line currents may be used for the relative location of voltage sag sources. The criteria are based on changes in the magnitude and/or angle of currents.	E-CBM	PB	[18, 21]	$\Delta\lvert I^{+}\rvert > 0$ and $\Delta\angle I^{+} < 0$	(5.1)
		IB	[31]	$\int_{0}^{t} \Delta\lvert i^{+}\rvert dt > 0$ and $\int_{0}^{t} \Delta\angle i^{+}dt < 0$	(5.2)
	E-PCSC	PB	[20]	$\Delta\angle I^{+} < 0$	(6.1)
		IB	[31]	$\int_{0}^{t} \Delta\angle i^{+}dt < 0$	(6.2)

extracted during the steady-state and especially within the transient period. Note that the E-RCC (PB) method is basically based on the first detected peak, which shows the importance of FLP for detecting sag sources. On the other hand, IB existing methods are based on the integral of the changes to filter the alternating component in the response. Furthermore, all the existing methods require the calculation of the changes due to voltage sag, i.e., $\Delta(.) = (.)_{sag} - (.)_{presag}$, where $(.)_{sag}$ includes the values after starting sag, while the values of $(.)_{presag}$ are obtained by extending and repeating the values for the last pre-sag cycle [23]. The real-life voltage sags are not a pure sinusoidal signal and, as such calculation of $\Delta(.)$ requires detection of the exact sag starting time, which is questionable for real-time applications. Hence, to increase the effectiveness and enhance the computations suitable for real-time applications, we propose several modifiers to the existing methods used within the transient period. FLP is a basic modifier that can increase effectiveness; however, applying it to the integral-based methods would make no sense. Therefore, using Mean or Trend instead of the integral will completely remove the alternating component in the response. Mean, and Trend can also be applied to PB methods. Moreover, a zero-mean (zm) signal, in which the mean value (one cycle sliding window) of a signal is removed, can be used instead of $\Delta(.)$, which does not require detection of the exact sag starting time. Furthermore, a Trend applies on a signal which includes values before and after the sag, (instead of $\Delta(.)$). In this way, five modifiers are proposed; Mean on signal changes, FLP on signal changes, Mean-zm on zero-mean signal, FLP-zm on zero-mean signal, and Trend of signals' trajectories versus time.

By applying the five modifiers on methods E-DPE, E-RCC, E-DR, E-CBM, and E-PCSC (PB/IB), new enhanced methods: M-DPE, M-RCC, M-DR, M-CBM, and M-PCSC (all PB/IB) are proposed. Therefore, each existing method can have five different modified methods applicable for the transient period of sag beginnings. Fig. 1 shows the employment steps of the modifiers to develop proposed new methods. The criteria *F/Fa/Fb* (for PB categories) and *f/fa/fb* (for IB categories) used by each new method are given in Table 2. The mean value applied in the last stage for the modifiers in Fig. 1 is the average of the criteria used for a half/one cycle period at the beginning of the voltage sag. The starting time of the variations due to sags in this study is considered according to the event's starting time for faults and TE. Hence, the inception time is already available in the simulations and field measurements. Before $t = 0$ is considered pre-sag, and, after that, as during sag.

In the end, the new methods with the highest accuracy and shortest time are suggested, which will be called selected modified methods. The selected methods, along with a fast and accurate voltage sag/fault inception time detection algorithm such as [50], are endorsed for real-time usages.

Amongst the selected methods, the methods with modifiers of Mean-zm and FLP-zm do not need the sag starting time detection, because a continuous subtracting of the mean value is being calculated. The extensive simulations have shown that shifting the transient time window around the sag starting time also does not affect the sign of the slope of signals' trajectories for the Trend modifier. Therefore, the selected methods with modifiers of Mean-zm, FLP-zm, and Trend will be highly recommended to be applied in real-time.

The application of proposed modifiers for formulating the US/DS rules for the new methods are given in Table 3 by (7.1.a) to (11.2.e), which apply for the transient period, i.e., half to one cycle after sag starting. The E-SST method will not be considered since it is sensitive to the selection of cycles during sags, and it does not have any potential to be improved considering transient periods of sags.

An example is shown in Fig. 2 for a voltage sag event due to a US line-to-line fault. This example states the shortfall of E-PCSC (PB) in the half-cycle time window, which wrongly shows a DS direction (Fig. 2c) when F is $\angle I^{+}$. According to new methods M-PCSC (11.1.a) and (11.1.b) (Mean and FLP modifiers shown in Fig. 2c), and the M-PCSC (11.1.c) and (11.1.d) (Mean-zm and FLP-zm modifiers shown in Fig. 2d), and M-PCSC (11.1.e.) (Trend modifier shown in Fig. 2e), all show positive signs in a short 0.5 cycle period, which confirm a correct US direction and a modification for E-PCSC (PB). Therefore, the new methods are accurate within the transient period of voltage sag beginning (i.e., more accurate and faster response).

4. Evaluation of the methods

4.1. Test power network

The simulated case study is based on an existing regional power network in the Mato Grosso state of Brazil [40] (60 Hz), as shown in Fig. 3. This real network has been modelled by PSCAD/EMTDC, and the output data were processed via MATLAB codes in a sampling frequency of 7.68 kHz. The PQMs were installed in 6 points (lower voltage side of

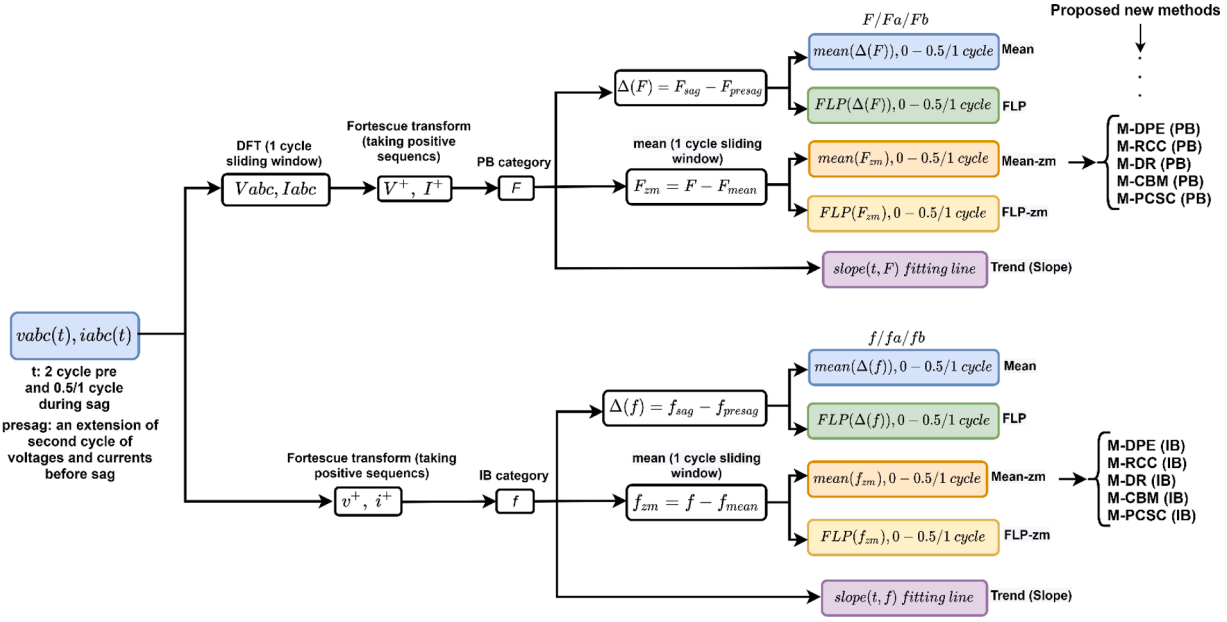

Fig. 1. Employment of the proposed modifiers for developing new methods.

Table 2
Criteria used by each proposed new method related to Fig. 1.

Proposed new methods	M-DPE		M-RCC		M-DR				M-CBM				M-PCSC	
Category	PB	IB	PB	IB	PB		IB		PB		IB		PB	IB
Used criterion	F	f	F	f	Fa	Fb	fa	fb	Fa	Fb	fa	fb	F	f
	P^+	p^+	$I^+cos(\theta)^+$	$i^+cos(\theta)^+$	$\lvert Z^+\rvert$	$\angle Z^+$	$\lvert z^+\rvert$	$\angle z^+$	$\lvert I^+\rvert$	$\angle I$	$\lvert i^+\rvert$	$\angle i^+$	$\angle I^+$	$\angle i^+$

Table 3
Proposed new methods for voltage-sag source detection for windows of half and one cycle after starting sag (F/Fa/Fb are extracted from Table 2).

Method	Modifier	PB basic rule for DS direction (else US)	(Eq.)	IB basic rule for DS direction (else US)	(Eq.)
M-DPE	Mean	$mean(\Delta F) > 0$	(7.1.a)	$mean(\Delta f) > 0$	(7.2.a)
	FLP	$FLP(\Delta F) > 0$	(7.1.b)	$FLP(\Delta f) > 0$	(7.2.b)
	Mean-zm	$mean(F_{zm}) > 0$	(7.1.c)	$mean(f_{zm}) > 0$	(7.2.c)
	FLP-zm	$FLP(F_{zm}) > 0$	(7.1.d)	$FLP(f_{zm}) > 0$	(7.2.d)
	Trend	$slope(t,F)\ line > 0$	(7.1.e)	$slope(t,f)\ line > 0$	(7.2.e)
M-RCC	Mean	$mean(\Delta F) > 0$	(8.1.a)	$mean(\Delta f) > 0$	(8.2.a)
	FLP	$FLP(\Delta F) > 0$	(8.1.b)	$FLP(\Delta f) > 0$	(8.2.b)
	Mean-zm	$mean(F_{zm}) > 0$	(8.1.c)	$mean(f_{zm}) > 0$	(8.2.c)
	FLP-zm	$FLP(F_{zm}) > 0$	(8.1.d)	$FLP(f_{zm}) > 0$	(8.2.d)
	Trend	$slope(t,F)\ line > 0$	(8.1.e)	$slope(t,f)\ line > 0$	(8.2.e)
M-DR	Mean	$mean(\Delta Fa) < 0$ and $mean(\Delta Fb) > 0$	(9.1.a)	$mean(\Delta fa) < 0$ and $mean(\Delta fb) > 0$	(9.2.a)
	FLP	$FLP(\Delta Fa) < 0$ and $FLP(\Delta Fb) > 0$	(9.1.b)	$FLP(\Delta fa) < 0$ and $FLP(\Delta fb) > 0$	(9.2.b)
	Mean-zm	$mean(Fa_{zm}) < 0$ and $mean(Fb_{zm}) > 0$	(9.1.c)	$mean(fa_{zm}) < 0$ and $mean(fb_{zm}) > 0$	(9.2.c)
	FLP-zm	$FLP(Fa_{zm}) < 0$ and $FLP(Fb_{zm}) > 0$	(9.1.d)	$FLP(fa_{zm}) < 0$ and $FLP(fb_{zm}) > 0$	(9.2.d)
	Trend	$slope(t,Fa)\ line < 0$ and $slope(t,Fb)\ line > 0$	(9.1.e)	$slope(t,fa)\ line < 0$ and $slope(t,fb)\ line > 0$	(9.2.e)
M-CBM	Mean	$mean(\Delta Fa) > 0$ and $mean(\Delta Fb) < 0$	(10.1.a)	$mean(\Delta fa) > 0$ and $mean(\Delta fb) < 0$	(10.2.a)
	FLP	$FLP(\Delta Fa) > 0$ and $FLP(\Delta Fb) < 0$	(10.1.b)	$FLP(\Delta fa) > 0$ and $FLP(\Delta fb) < 0$	(10.2.b)
	Mean-zm	$mean(Fa_{zm}) > 0$ and $mean(Fb_{zm}) < 0$	(10.1.c)	$mean(fa_{zm}) > 0$ and $mean(fb_{zm}) < 0$	(10.2.c)
	FLP-zm	$FLP(Fa_{zm}) > 0$ and $FLP(Fb_{zm}) < 0$	(10.1.d)	$FLP(fa_{zm}) > 0$ and $FLP(fb_{zm}) < 0$	(10.2.d)
	Trend	$slope(t,Fa)\ line > 0$ and $slope(t,Fb)\ line < 0$	(10.1.e)	$slope(t,fa)\ line > 0$ and $slope(t,fb)\ line < 0$	(10.2.e)
M-PCSC	Mean	$mean(\Delta F) < 0$	(11.1.a)	$mean(\Delta f) < 0$	(11.2.a)
	FLP	$FLP(\Delta F) < 0$	(11.1.b)	$FLP(\Delta f) < 0$	(11.2.b)
	Mean-zm	$mean(F_{zm}) < 0$	(11.1.c)	$mean(f_{zm}) < 0$	(11.2.c)
	FLP-zm	$FLP(F_{zm}) < 0$	(11.1.d)	$FLP(f_{zm}) < 0$	(11.2.d)
	Trend	$slope(t,F)\ line < 0$	(11.1.e)	$slope(t,f)\ line < 0$	(11.2.e)

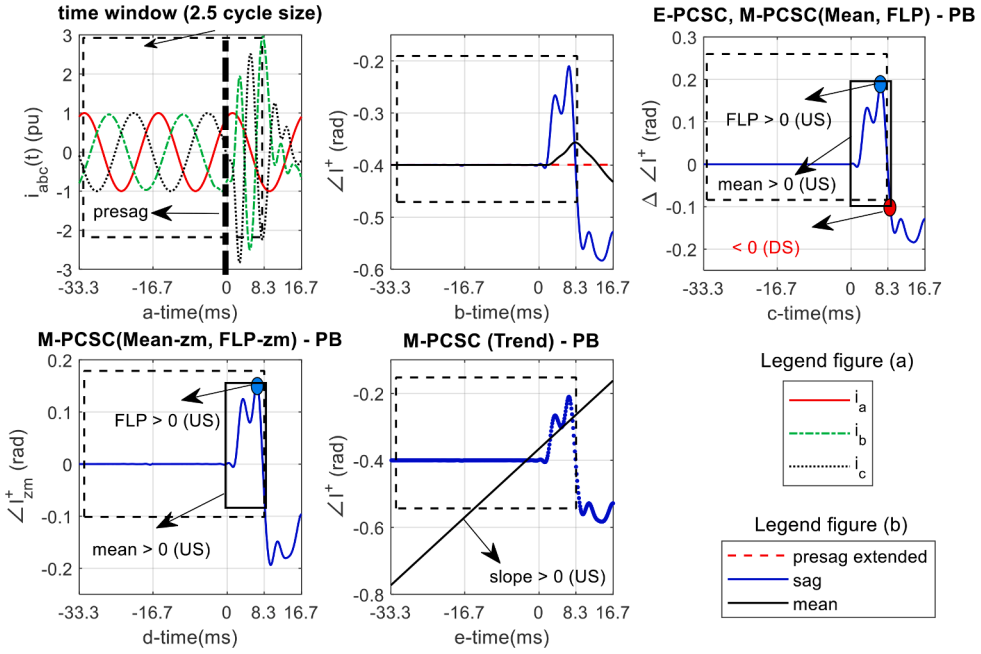

Fig. 2. Voltage sag event due to a US LL fault (a) Line currents; (b) Angle of positive-sequence current; (c) Results of E-PCSC (PB), M-PCSC (11.1.a) and M-PCSC (11.1.b); (d) Results of M-PCSC (11.1.c) and M-PCSC (11.1.d); (e) Results of M-PCSC (11.1.e).

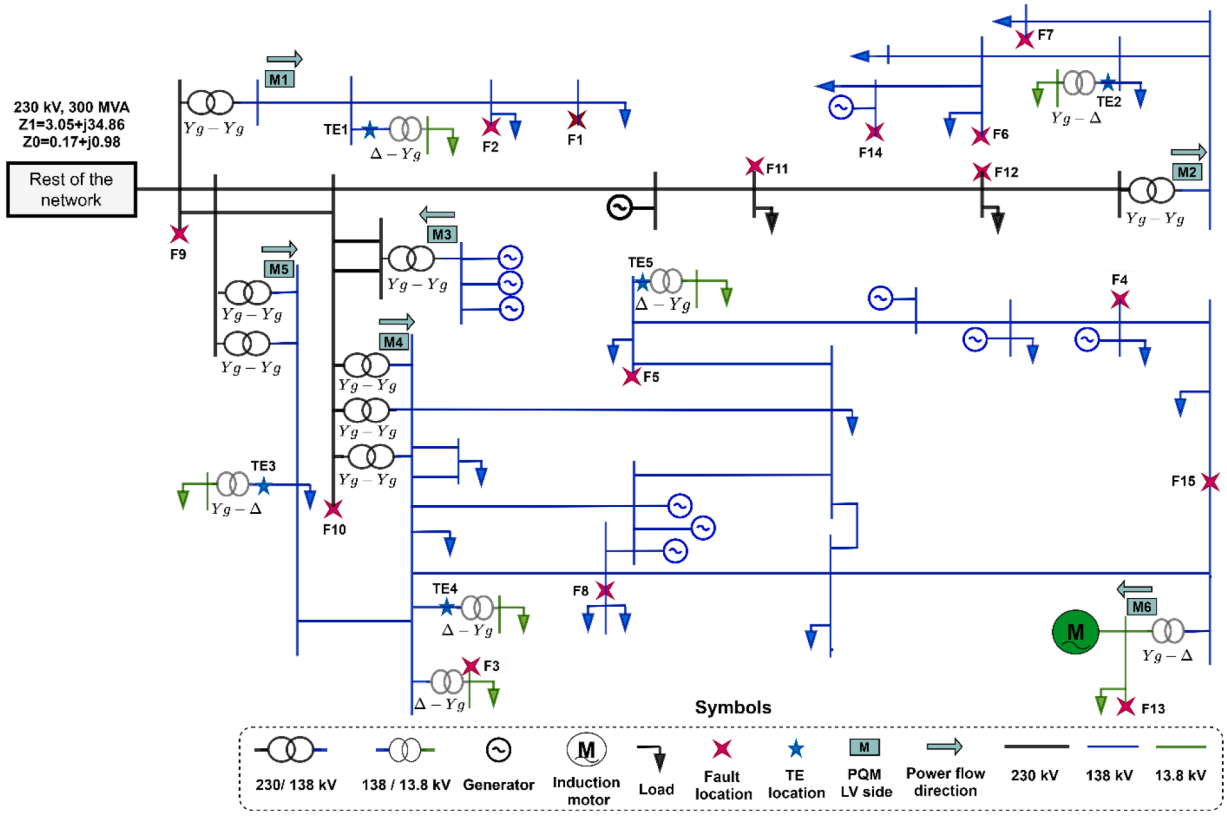

Fig. 3. Testing network for numerical simulations of voltage sags due to faults and TEs.

power transformers), with M1 at a 138 kV line, M2…M5 on the boundary between the 230 and 138 kV networks and M6 between the 138 kV and 13.8 kV networks. DS/US directions are related to pre-voltage sag active power flow direction. The loads are, typically, constant impedance, constant power and induction motors. Various faults with 100 ms duration (a typical fault clearing time in transmission networks) are simulated under different system conditions such as: 15 fault locations (F1 … F15), 11 fault types (LLLG, LLL, LG-a, LG-b, LG-c, LLG (LL)-ab, LLG (LL)-bc, LLG (LL)-ca), 5 fault impedances (Rf= 0.001, 1, 10, 40 and 80 Ω) and 6 PQMs installed over the different typologies of networks (M1 … M6). Consequently, $15 \times 11 \times 5 = 825$ fault cases were obtained and evaluated in the 6 PQMs, totalling 4950 samples, which 1826 of them were voltage sags (occurrence average of 2.2 Vage sag per fault). Five TE points were simulated (TE1…TE5) with 7 different transformer capacities, hence $5 \times 7 \times 6 = 210$ TE samples were obtained, of which 166 were voltage sags. The fault and TE cases were used to test the detection methods.

4.2. Results of existing methods in the transient and steady-state periods

This section will conclude that: (a) some methods work better if they are employed during a transient period and not during a steady-state period (b) some other methods are hindered during a transient period and need to be improved. Extensive simulations for sags with different time durations (even less than 100 ms) have shown that the transient period of sags normally occurs for a window of less than one cycle. Hence, different time windows are selected as half and one cycle for a transient period and two, three, and six cycles for the steady-state period denoted by markers. The criterion "sign" for each method during all different time windows is shown on the top of each Figure because, according to Table 1, the "sign" of criterion and not "numerical value" shows the direction of sag sources. Special attention is paid to the half and one-cycle time windows, where the wrong result, which will be improved by proposed modified methods, is also marked by an arrow. The results of existing methods applied to locate sag sources (fault and TE) as (DS/US) are shown in Figs. 4–11.

In Fig. 4a, the E-DPE (PB) method shows a correct DS direction because of the positive sign of energy for only half and one-cycle time windows, +0.0014 pu, and +0.0022 pu, respectively, due to a DS symmetrical fault (1.1). E-DPE (IB) indicates the true direction for only a half cycle time window (the energy is +0.0023 pu), while the wrong performance of the one-cycle window (the energy is −0.0009 pu) is shown by an arrow (1.1). Therefore, E-DPE (IB) could be improved by the proposed modifiers. The half-cycle window is the only one in which E-RCC (PB) (2.1) and (IB) (2.2) methods have a correct positive value (sign) for locating a DS TE, as shown in Figs. 5b and d, respectively. The E-RCC (PB) (Fig. 5b) wrongly shows a US direction for a one-cycle window. Therefore, E-RCC also may need to be improved to detect sag sources during a transient period. In Figs. 6b and d, the E-SST (PB) (3.1) and (IB) (3.2) methods have shown a correct DS direction due to negative sign of slope, which is related to a DS TE for the half and one-cycle windows, respectively.

Positive changes of impedance angle during the half-cycle window shown in Figs. 7a and d for E-DR (PB) (4.1) and (IB) (4.2) methods indicate an incorrect DS direction for a voltage sag source (a US asymmetrical fault). The wrong direction of E-DR (IB) will be corrected by the proposed modifiers. Time responses of E-CBM (PB) (5.1) in Figs. 9a and b, and E-CBM (IB) (5.2) in Figs. 9c and d are related to a US asymmetrical fault. The methods indicate a correct DS direction in all different time windows except for the half-cycle window. The proposed modifiers will improve the performance of E-CBM. The current angle changes for a voltage sag due to a US asymmetrical fault are shown in Figs. 11a (for E-PCSC (PB)) (6.1) and c (for E-PCSC (IB)) (6.2). The E-PCSC (PB) has failed for all different time windows due to negative current angle changes. The E-PCSC (IB) returns a correct result only during the half-cycle time window while fails for the one-cycle window. Therefore, E-PCSC also needs improvement.

The effectiveness of existing methods during different time windows

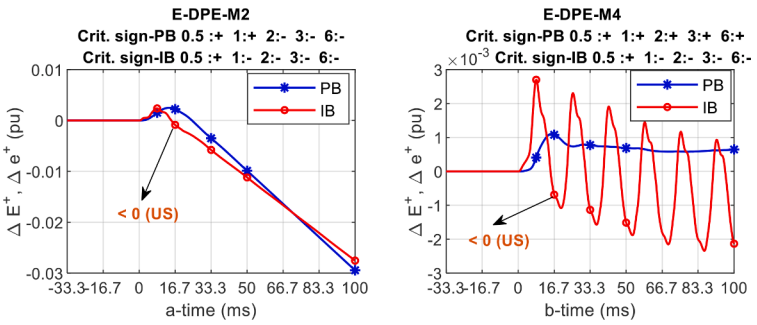

Fig. 4. Numerical simulations of E-DPE methods for a sag (An arrow means new modified methods will improve the performance) (a) Due to a DS symmetrical fault (F6); (b) Due to a DS TE (TE5).

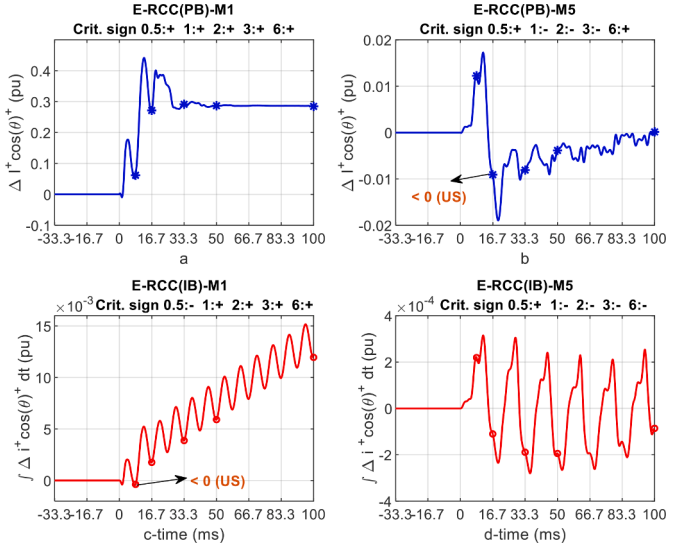

Fig. 5. Numerical simulations of E-RCC methods for a sag (a), (c) Due to a DS earth fault-b (F1); (b), (d) Due to a DS TE (TE5).

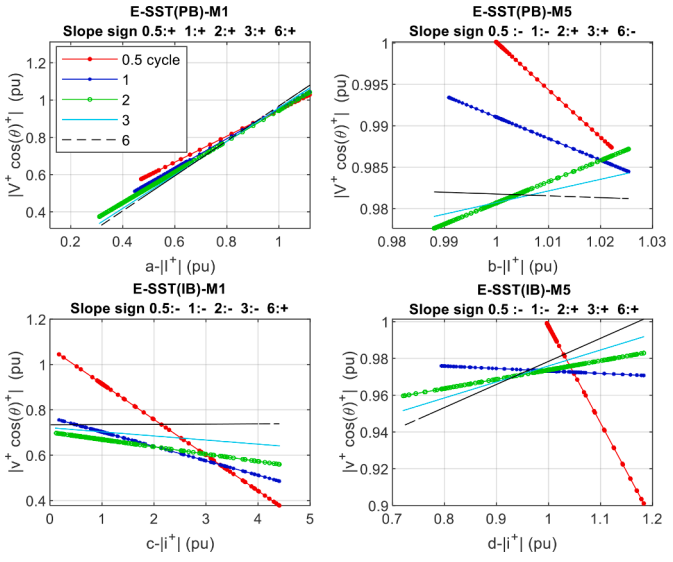

Fig. 6. Numerical simulations of E-SST methods for a sag (a), (c) Due to a US asymmetrical fault-bc (F10); (b), (d) Due to a DS TE (TE4).

for all simulated voltage sags is shown in Fig. 12. Throughout this paper, performance/effectiveness is defined as the number of correct results per total number of fault/TE cases. Fig. 12a is related to 1826 sags due to

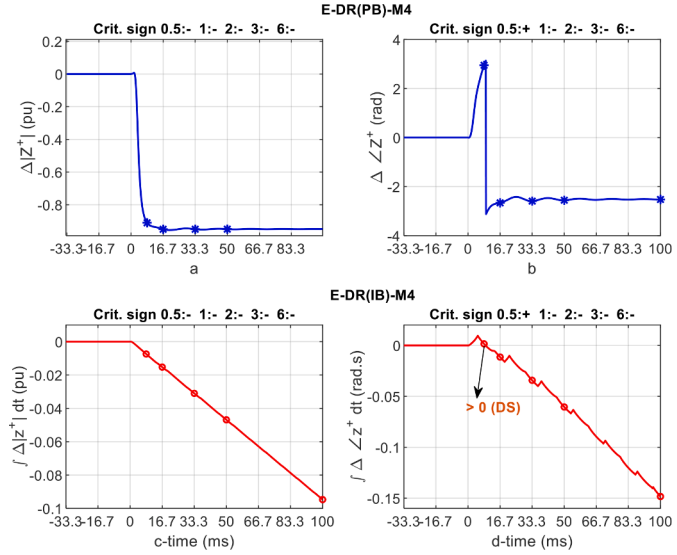

Fig. 7. Numerical simulations of E-DR methods for a sag Due to a US asymmetrical fault-ca (F9) (a), (b) PB magnitude and angle change; (c), (d) IB magnitude and angle change.

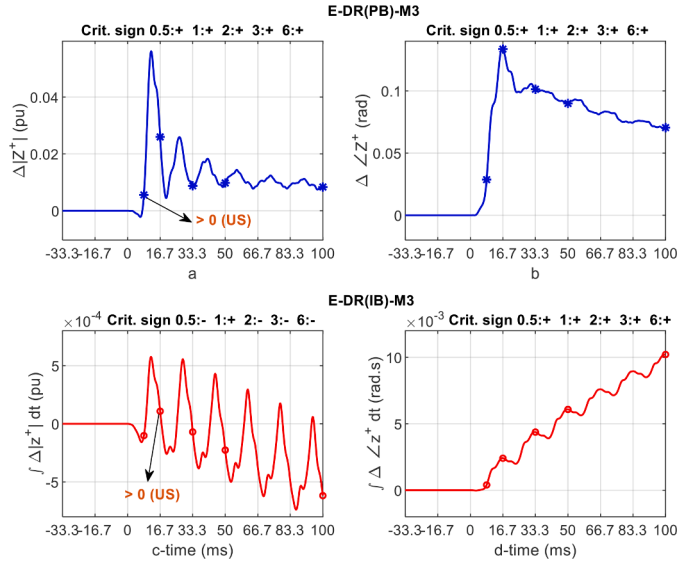

Fig. 8. Numerical simulations of E-DR methods for a sag Due to a DS TE (TE3) (a), (b) PB magnitude and angle change; (c), (d) IB magnitude and angle change.

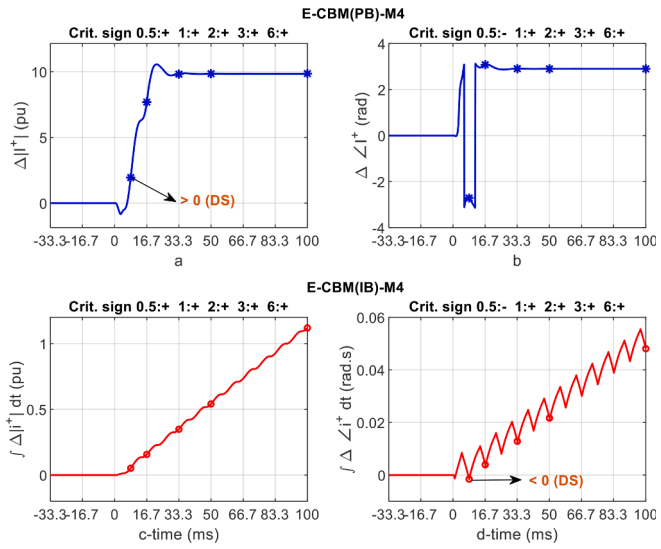

Fig. 9. Numerical simulations of E-CBM methods for a sag due to a US asymmetrical fault-bc (F10) (a), (b) PB magnitude and angle change; (c), (d) IB magnitude and angle.

faults, and Fig. 12b is for 166 sags due to TE. Fig. 12 shows that all methods have better effectiveness in PB category for sags due to faults (white bars in Fig. 12a). For example, the values for E-CBM: Half cycle (85.1% (PB) > 78.3% (IB)), one cycle (93.8% (PB) > 84.2% (IB)), two cycles (95.5% (PB) > 86.1% (IB)), three cycles (95.5% (PB) > 87.2% (IB)), and six cycles (95.3% (PB) > 90.5% (IB)).

However, for the short duration sags and/or sags due to transient sources [30, 31], the methods with the IB category may have better performance. Sags, due to TE, are good candidates for methods with the IB category. This is so because of the second-order harmonic of current signals on the TE events (grey bars in Fig. 12b).

For example, the values for E-DPE: Half cycle (86.8% (PB) < 96.4% (IB)), one cycle (79.5% (PB) > 78.3% (IB)), two cycles (79.5% (PB) < 84.9% (IB)), three cycles (79.5% (PB) < 85.5% (IB)), six cycles (81.3% (PB) < 85.5% (IB)), in which all windows have shown better performance for IB methods, except the half-cycle window for which the PB and IB methods are almost similar.

Observations for employing the existing methods during transient periods of sags (time window of half and one-cycle) in comparison to two, three, and six cycles (steady-state period), are as follows:

***For fault cases*:** The accuracy of E-DPE and E-RCC methods has been increased when employed in a transient period. For example, E-DPE (PB) shows an accuracy of 98.2% (half cycle) and 95.2% (one cycle), which is higher than the accuracy in other windows, i.e., 90.9% (two cycles), 89.4% (three cycles), and 88.1% (six cycles). However, methods E-DR, E-CBM, and E-PCSC do not perform at a good enough need to be improved. For example, E-CBM (IB) shows an accuracy of 78.3% (half cycle) and 84.2% (one cycle), which is lower than the accuracy in other windows, i.e., 86.1% (two cycles), 87.2% (three cycles), and 90.5% (six cycles). These results show the necessity of proposed modifiers to enhance the performance of E-DR, E-CBM, and E-PCSC methods and maintain the increased accuracy of others.

***For TE cases*:** Methods DPE (IB) (96.4%), E-RCC (IB) (95.2%), E-DR (IB) (100%), E-CBM (IB) (100%), and E-PCSC (IB) (100%) have shown very high accuracy for the half-cycle time window, which shows that the methods do not need improvement and they are fast and accurate. However, PB methods must be enhanced for half and one-cycle windows, which shows again the importance of applying the proposed modifiers.

By employing the E-SST method in a transient period, its maximum accuracy was obtained for a one-cycle window, 82.3% for PB (fault cases) and 83.1% for IB (TE cases). Still, the method will not be considered in our modifications since it is based on the slope of voltage variations versus a current variation.

4.3. Results of proposed new methods in the transient period

In order to evaluate the new modified methods for half and one-cycle time windows, the sag cases shown in Figs. 4- 11 (indicated by arrows) were analysed by modified methods, as shown in Figs. 13- 15. To better understand the enhanced methods, the time axes are shown for a quarter cycle before sag and half/one cycle during sag. The cases that caused the existing methods to fail and were explained in Section 4.2 are now described.

A value of FLP = +0.69 on Δp^+ (Fig. 13a) by M-DPE (7.2.b) correctly shows a DS direction for a fault in a one-cycle window, which improves E-DPE (IB) shown in Fig. 4a.

A value of Mean = 0.005 pu (M-RCC (8.1.a)) and FLP = 0.018 pu (M-RCC (8.1.b)) on $\Delta I^+cos(\theta)^+$ (Fig. 14j), a value of Mean = +0.003 pu (M-RCC (8.1.c)) on $I^+cos(\theta)^+_{zm}$ (Fig. 14k), and the slope of the line $(t, I^+cos(\theta)^+)$ as +0.3 by M-RCC (8.1.e) (Fig. 14l) correctly locate a DS TE source in the one-cycle window. This correct location of the sag source is an improvement of E-RCC (PB) shown in Fig. 5b.

Negative values of impedance angle, in a half-cycle window, used as the criterion of M-DR (9.2.c) and M-DR (9.2.d) shown in (Fig. 13e) (Mean-zm = −0.75 rad, FLP-zm = −4.22 rad), and M-DR (9.2.e) (Slope = −105) shown in (Fig. 13g), locate a US fault. The correct location of the fault is obtained due to the proposed improvement of E-DR (IB) shown in Fig. 7d.

All five modifiers obtained during the half-cycle time window applied to E-CBM (PB) result in M-CBM (10.1.a) to (10.1.e). The M-CBM correctly locates a US fault, as seen in Figs. 13h to m. The true US direction is obtained due to the improvement of E-CBM (PB) seen in Figs. 9a and b. The positive sign of current angle in the half-cycle time window for M-CBM (10.1.c) (Mean-zm = +1.61 rad) and (10.1.d) (FLP-zm = +2.91 rad) in Fig. 13k and M-CBM (10.1.e) in Fig. 13l (Slope = +23) correctly locates a US fault. On the other hand, the E-CBM (IB) wrongly defined a DS direction (Figs. 9c and d).

Figs. 14b to g show that the M-PCSC (11.1.a) to (11.2.e) correctly located an US fault. The positive current angle has been a verification of the improvement related to Fig. 11a for a half-cycle window and Fig. 11c for a one-cycle window.

Some of the failures of both existing and modified methods in a defined transient period of sags are explained here. E-CBM (IB) shown in Fig. 10c, M-CBM (10.2.a) and (10.2.b) shown in Fig. 15k, M-CBM (10.2.c) and (10.2.d) shown in Fig. 15l, as well as M-CBM (10.2.e) shown in Fig. 15m present a negative current magnitude in a one-cycle time window which wrongly locates a US direction for a DS TE case. However, as shown in Fig. 12, utilization of IB existing methods in a transient period of half-cycle has resulted in a good performance for TE sources. Therefore, there was no need to improve the methods for a one-cycle window because a good response already exists in a shorter time window.

All existing methods (Table 1) and proposed new ones (Table 3) were tested and analysed for all voltage sag cases, considering voltage and current transient signals. The effectiveness of methods is shown in Table 4 for 1826 sags due to different fault cases and Table 5 for 166 sags due to TE cases. As said in Section 4.2, only the PB methods are tabulated here in Table 5. As shown in Tables 4 and 5, we have considered four scenarios to check how accurate are the modified methods considering transient signals from half and one-cycle time windows separately, as follows:

Scenario 1: "increased" effectiveness by modified methods is "a little less" than the effectiveness of the existing method over other time windows (shown by ↑); for example, M-DR (9.1.c) (FLP modifier) has an accuracy of 89% for the 0.5 cycle window, which is higher than E-DR (4.1) with the accuracy of 85%. However, this "increased" effectiveness

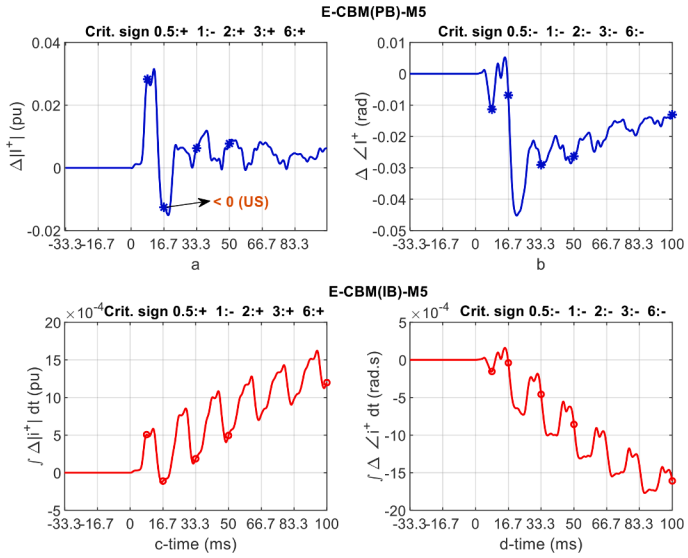

Fig. 10. Numerical simulations of E-CBM methods for a sag due to a DS TE (TE4) (a), (b) PB magnitude and angle change; (c), (d) IB magnitude and angle change.

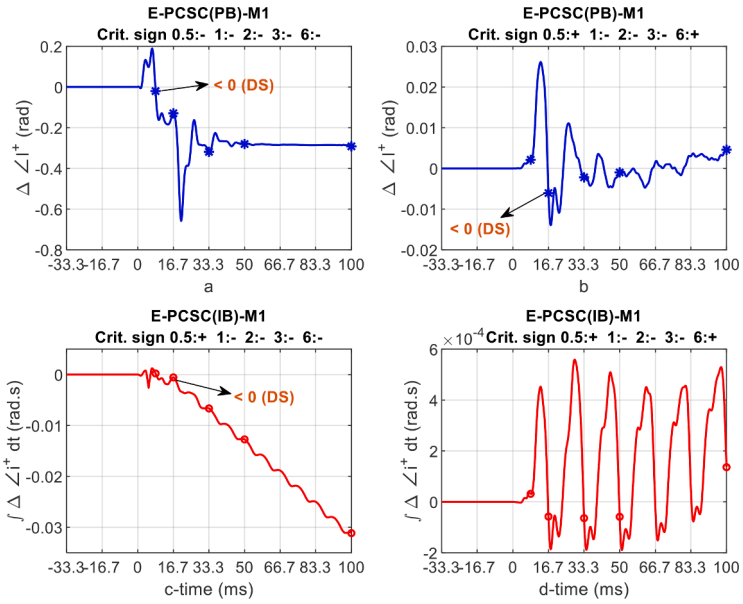

Fig. 11. Numerical simulations of E-PCSC methods for a sag (a), (c) Due to a US asymmetrical fault-bc (F10); (b), (d) Due to a US TE (TE2).

is a little less than the accuracy of E-DR (4.1) over the windows of one cycle (90.9%) and two cycles (90.1%) (see Table 4 for M-DR (9.1.c) and Fig. 12a E-DR (4.1)).

Scenario 2: "increased" effectiveness by modified methods is "higher/equal" than the effectiveness of the existing method over all time windows (shown by ⇑); for example, M-RCC (8.1.e) (Trend modifier) has a perfect accuracy (100%) for the one-cycle window, which is higher than E-RCC (2.1) over all time windows as: Half cycle (99.6%), half cycle (97%), two cycles (96.3%), three cycles (95.1%), six cycles (95.4%) (see Table 4 for M-RCC (8.1.e) and Fig. 12a E-RCC (2.1)).

Scenario 3: This scenario is about the cases in which applying existing methods within a half or one-cycle window has increased (or hasn't changed) their effectiveness compared to other time windows of steady-state period. Therefore, *Scenario 3* keeps the increased/same effectiveness of existing methods by modified ones, which confirm the properness of our proposed modifiers (shown by ∘). For example, Fig. 12a shows that E-DPE (1.2) has an accuracy of 92% for the half-cycle window, which is higher than all other time windows, such as one cycle (89.3%), two cycles (88.5%), three cycles (87.7%), six cycles (87.1%). Table 4 shows that M-DPE (7.2.a) (Mean modifier) keeps the 92%, which was obtained for the E-DPE (1.2) within the half cycle window.

Scenario 4: Decreased effectiveness of the modified methods (shown by —); this scenario is related to a few of the modifiers which couldn't improve the existing methods; therefore, they are not mentioned in Tables 4 and 5.

A selection has been done amongst the new modified methods in order to choose the most accurate time window (half or one cycle) according to the four considered scenarios. The final selection criteria are developed as follows: If (effectiveness of 1 cycle > effectiveness of 0.5 cycle), then the selected method is the method that uses 1 cycle. If the tolerance for smaller effectiveness of 0.5 cycle is –5%, then the method of 0.5 cycle will also be selected. If (effectiveness of 0.5 cycle ≥ effectiveness of 1 cycle), then the selected method is the one that uses 0.5 cycle.

In order to show how the selected method obtains for the cases of scenario 4, an example is given here: the 0.5 cycle effectiveness of M-DR

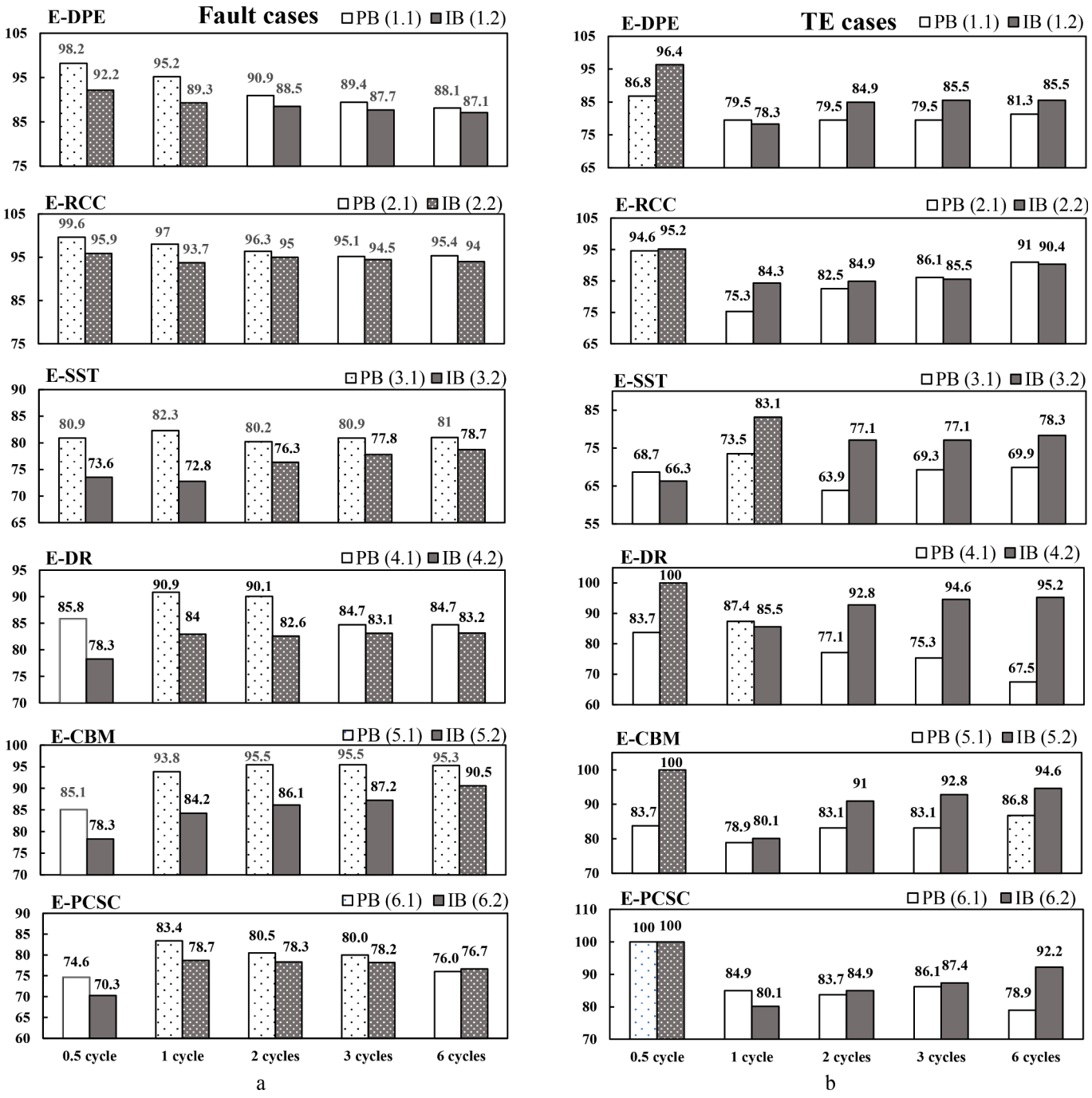

Fig. 12. Effectiveness of existing methods (Table 1) in (%) during different time windows of 0.5, 1, 2, 3, and 6 cycles for both fault and TE cases. Highlighted as dotted is the maximum effectiveness shown for each method (a) Voltage sags due to faults; (b) Voltage sags due to TEs.

(9.1.a) is decreased (—); therefore 1 cycle M-DR (9.1.a) (91%) is compared with the highest accuracy of its own 1 cycle modifier ((9.1.e)) (96%). Since 91% is smaller than 96%, the 1 cycle M-DR (9.1.a) is not selected. If it was higher or equal, it would be selected.

The selected modified methods are indicated by a tick (✓), and the best of each method is highlighted in blue in Tables 4 and 5. The IB methods for a 0.5 cycle window must be added to Table 5 since their performance is already good, as shown in Fig. 12b.

Table 6 shows that the largest effectiveness of the new selected methods is now obtained for a transient period of sags (half and one-cycle time windows). Hence, these methods have better performance for real-time applications, whereas the maximum accuracy of existing methods is spread over different time windows (see Fig. 12a).

Table 7 shows the best selected modified analytical methods, related existing methods, and two supervised machine learning-based methods, i.e., support vector machine (SVM) with polynomial kernel and an ensemble learning on the decision tree learners by the TotalBoost aggregation method, for transient and steady-state periods. The results of intelligent methods are taken from reference [40], which has a similar case study.

As seen from Table 7, the accuracy has been perfect (100%) for some of the proposed selected methods (1st column), which is higher than machine learning-based methods (columns 4, 5, 7, and 8). An ensemble method reached 99.2% accuracy by feeding five optimum features in the best condition. Therefore, the best selected modified methods utilizing one or two features extracted from a transient period are more accurate

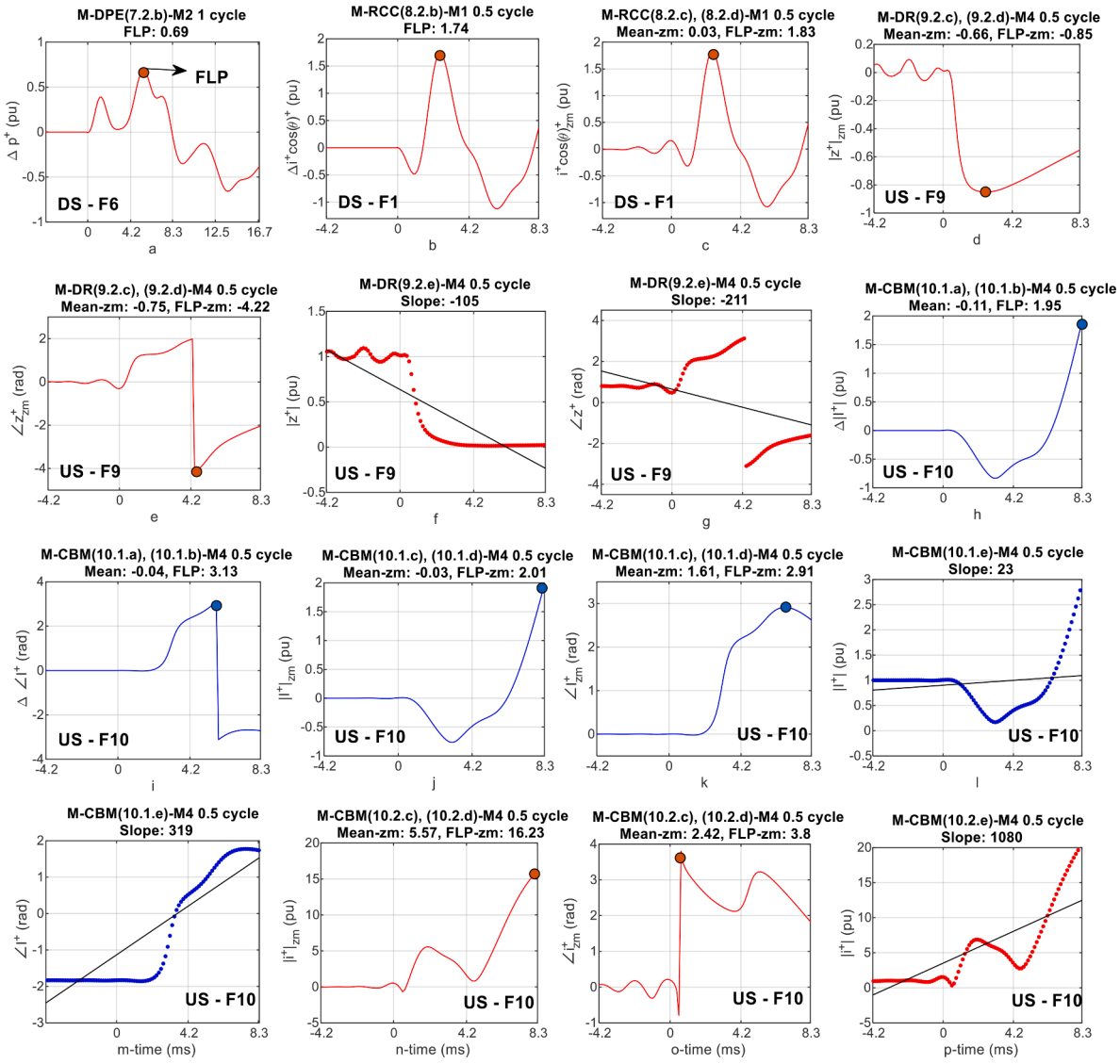

Fig. 13. Time responses obtained by the modified methods for the cases shown by arrows in Figs. 4(a), 5(c), 7(d), 9(a) and 9(d) for 0.5 or 1 cycle time window. Actual directions are shown inside the figures. Blue and red colors are related to PB and IB methods. FLP values are marked.

(100% accuracy) and faster than the ensemble learning method (99.2% accuracy), which needs five features extracted from a steady-state period. Also, the training process of the intelligent methods in online applications is time-consuming. However, a more accurate and faster machine learning-based method can be built by employing the transient modified features (extracted from the methods highlighted in Table 4 and 5) applied to PB or IB intelligent methods. From column 3 back to 1 in Table 7, the increased accuracy of the existing methods is shown, due to employing them in the transient period and also improving by the proposed selected method.

5. Field-testing results

This section introduces the field testing developed to verify the performance of the methods to locate voltage sag sources. As given in Table 8, fifteen field tests were applied to both existing and new selected modified methods (shown by ✓ in Tables 4 and 5). Line currents were captured through measurement devices installed at substations and over the lines within a Slovenian power network at different voltage levels with different sampling frequencies.

In order to highlight the improvement of the proposed selected modified methods (shown by ✓ in Tables 4 and 5) over the previous ones, for half and one-cycle time windows, three examples of the field-testing results are shown in Fig. 16 (currents and voltages measurements), Figs. 17 and 18 (existing methods with incorrect results), and Fig. 19 (improved results by selected modified methods extracted from Tables 4 and 5). Regarding SM-DR and SM-CBM methods, the failed criterion of the related existing methods, which was improved by modifiers (i.e., magnitude and/or angle), are shown in Fig. 19. Those three examples are from Test 1, a 0.22 pu sag on a 20 kV distribution feeder recorded by protection relays due to a DS LG-a fault in a low resistance earthing's network (Figs. 16a and b); Test 8, a 0.82 pu sag on 110 kV level due to a US LL-bc fault (Figs. 16c and d); and Test 10 which is the result of TE measured on the primary side of a 20/0.4 kV transformer. Two cycles later, an extremely asymmetrical voltage sag was caused due to an unknown LL fault, which quickly developed into a LLL fault (Figs. 16e and f).

To detect the location where those three events originated, the time responses of E-DR (IB) (Fig. 17c) and E-CBM (PB) in addition to E-PCSC (PB) (Fig. 18a), E-CBM (IB), and also to E-PCSC (IB) (Fig. 18b) are investigated in half, one, two, three and five-cycle time windows for "Test 1″.

The magnitude and angle changes of impedance during a half-cycle window are positive and negative, respectively, and the angle changes

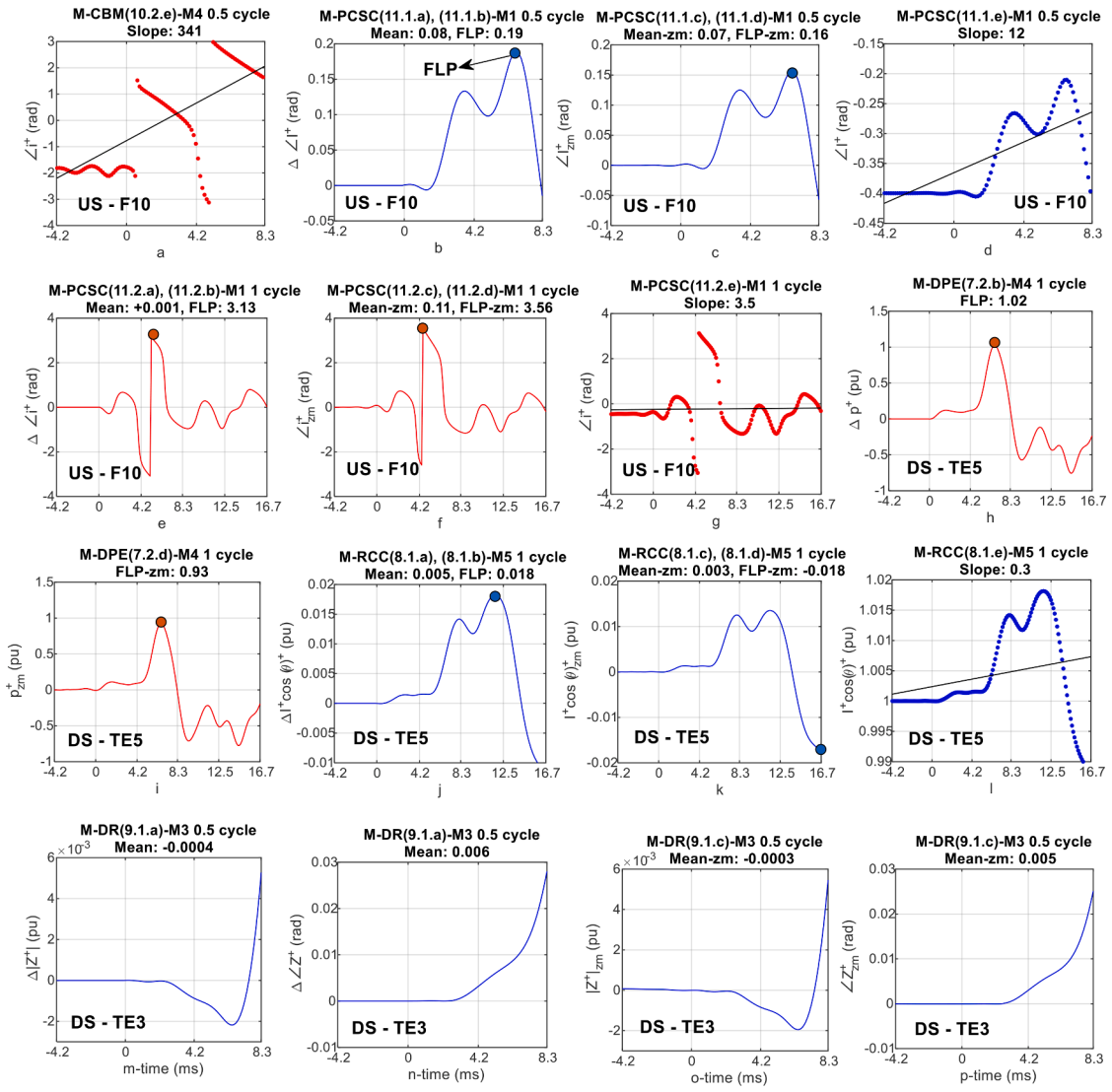

Fig. 14. Time responses obtained by the modified methods for the cases shown by arrows in Figs. 9(d), 11(a), 11(c), and TE similar cases shown by arrows in Figs. 4 (b), 5(b), 8(a), and 8(c) for 0.5 or 1 cycle time window. Actual directions are shown inside the figures. Blue and red colors are related to PB and IB methods, respectively. FLP values are marked.

are negative for the one-cycle window. Hence, an incorrect US source is detected by E-DR (IB). On the other hand, SM-DR (9.2.c), (9.2.d), and (9.2.e) correctly detect a DS fault by using a half-cycle window, as seen in Figs. 19c - f. The DS source detection results from negative and positive signs for impedance magnitude and angle. Figs. 19g - i show a positive impedance angle from SM-DR (9.2.a) to (9.2.e) for a one-cycle window, which confirms a DS source correctly.

The negative current angle changes are the reason for showing a wrong US direction instead of a DS source related to a half-cycle window for E-CBM (PB/IB) and E-PCSC (PB/IB) (Figs. 18a and b). Whereas SM-CBM and SM-PCSC shown in Figs. 19l and m (for PB category) and Figs. 19n and o (for IB category) result in a negative value of current angle, which indicates a DS source correctly using a half-cycle window.

The results of applying "Test 8″ (US direction) on the E-DPE (PB) and E-RCC (PB) for half, one, two, three, and four-cycle time windows are shown in Figs. 17a and 17b, respectively. Both methods failed for a half-cycle window because of the positive value of their own criterion. The SM-DPE (7.1.e) and SM-RCC (8.1.e) showed a negative slope which means a correct US direction, as seen in Figs. 19a and b.

In order to detect the TE event related to "Test 10″, consider the results obtained from E-DR (PB) (Fig. 17d), E-CBM (PB) and E-PCSC (PB) (Fig. 18c), and E-CBM (IB) and E-PCSC (IB) (Fig. 18d) for half, one and two-cycle time windows. The negative impedance angle changes yielded a wrong US TE for a one-cycle window (Fig. 17d). However, SM-DR (9.1.c) to (9.1.e) resulted in a positive impedance angle that correctly located a DS TE event, as shown in Figs. 19j and k. Positive signs of current angle in Figs. 18c and d detected an incorrect US TE for the one-cycle window. On the other hand, SM-CBM (PB) and SM-PCSC (PB) shown in Figs. 19p - r yielded a negative value of the current angle, confirming a true DS direction. Although the IB modified methods related to TE sources in a half-cycle window were not considered as selected, the SM-CBM and SM-PCSC had a negative current angle, which correctly resulted in a DS direction (Figs. 19s and t).

All field-testing results obtained by the discussed methods are shown in Tables 9 and 10 for half and one-cycle windows, respectively. The selected modified methods yield wrong results only when the existing methods have failed for all different windows (see Table 11), which normally concerns the earth faults with high earthing resistance, such as Tests 2 and 11. This confirms the effect of the neutral grounding resistance on voltage sags [52] and the zero-sequence component on the positive-sequence based methods. As seen in Table 8, the sag durations for the 15 fault cases are different, in which cases 6 – 19 include voltage sags with a period of less than 100 ms; therefore, the existing test cases for different time windows are:

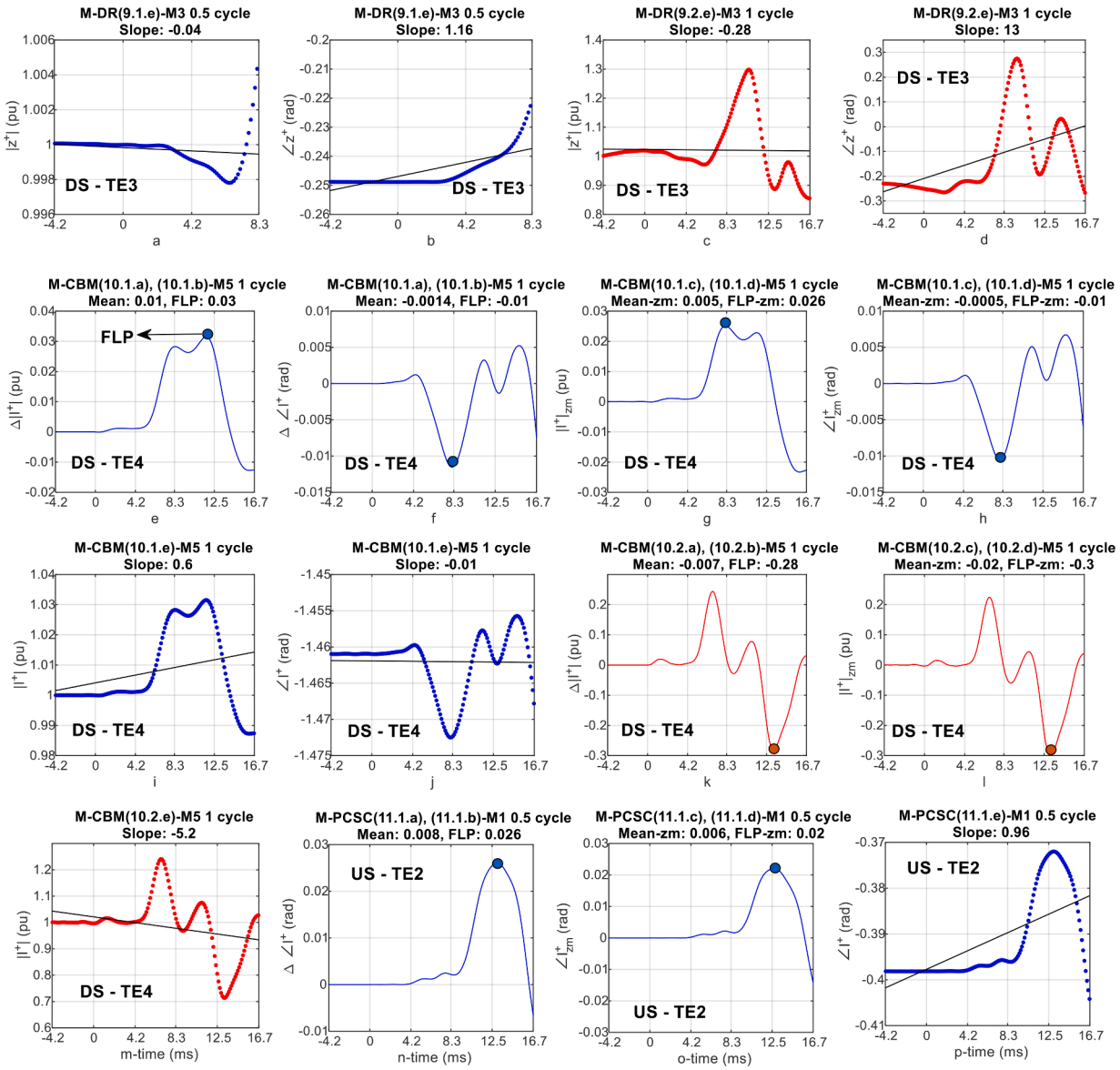

Fig. 15. Time responses obtained by the modified methods for the cases shown by arrows in Figs. 8(a), 8(c), 10(a), and 10(c) in 0.5 or 1 cycle time window and the modified PCSC methods for the US TE2 case shown by an arrow in Fig. 11(b) for 0.5 cycle time window. Actual directions are shown inside the figures. Blue and red colors are related to PB and IB methods. FLP values are marked.

Table 4
Effectiveness of existing, modified, and selected methods in (%) during the half and one-cycle time windows for fault cases.

Time window (cycle)	Type of method	Modifier	DPE		RCC		DR		CBM		PCSC	
			PB	IB	PB	IB	PB	IB	PB	IB	PB	IB
0.5	Existing	—	98	92	99.6	96	85	78	85	78	75	70
	Modified	Mean	**98** ∘✓	**92** ∘✓	99.4 ∘✓	**96** ∘✓	—	—	—	—	—	—
	Modified	FLP	**98** ∘✓	**92** ∘✓	99.8 ∘✓	**96** ∘✓	87 ↑	—	—	—	80 ↑✓	—
	Modified	Mean-zm	**98** ∘✓	91 ∘✓	99.3 ∘✓	**96** ∘✓	89 ↑✓	85 ⇑✓	92 ⇑✓	88 ↑✓	81 ↑✓	84 ⇑✓
	Modified	FLP-zm	**98** ∘✓	91 ∘✓	99.7 ∘✓	95 ∘✓	90 ⇑✓	87 ⇑✓	92 ⇑✓	89.8 ⇑✓	86 ⇑✓	84 ⇑✓
	Modified	Trend	**98** ∘✓	—	99.5 ∘✓	—	91 ⇑✓	83 ⇑✓	92 ⇑✓	90 ⇑✓	82 ↑✓	81 ⇑✓
1	Existing	—	95	89	97	93	91	84	94	84	83	79
	Modified	Mean	95 ∘	90 ↑	**100** ⇑✓	93 ∘	91 ∘	88.7 ⇑✓	—	—	83 ∘	79 ∘
	Modified	FLP	95 ∘	90 ↑	**100** ⇑✓	93 ∘	—	—	—	—	82 ∘✓	—
	Modified	Mean-zm	95 ∘	—	**100** ⇑✓	—	91 ∘✓	**90** ⇑✓	96 ⇑✓	**92** ⇑✓	83 ∘✓	**88** ⇑✓
	Modified	FLP-zm	—	—	**100** ⇑✓	—	91 ∘✓	—	96 ⇑✓	—	**90** ⇑✓	—
	Modified	Trend	—	—	**100** ⇑✓	—	**96** ⇑✓	84 ∘✓	**97** ⇑✓	—	87 ⇑✓	83 ⇑✓

↑: increased effect. < effect. of the existing related method for some of the time windows; ⇑: increased effect. ≥ effect. of the existing related method for all different time windows; ∘: (same effect. - 3%) ≥ effect. of the existing related method over all different time windows; —: decreased effect.; ✓: selected modified method; Bolded: best selected modified methods over each of the methods separately.

Table 5
Effectiveness of PB existing methods, modified and selected in (%) during the half and one-cycle time windows for TE cases.

Time window (cycle)	Type of method	Modifier	DPE	RCC	DR	CBM	PCSC
0.5	Existing	—	87	94	83	84	100
	Modified	Mean	**100**	**100**	90	84	—
	Modified	FLP	⇑✓	⇑✓	⇑✓	∘✓	**100**
	Modified	Mean-	98	98	—	—	∘✓
	Modified	zm	⇑✓	⇑✓	91	84	—
	Modified	FLP-zm	**100**	**100**	⇑✓	∘✓	99 ∘✓
		Trend	⇑✓	⇑✓	—	—	99 ∘✓
			99	99	89	85	
			⇑✓	⇑✓	⇑✓	⇑✓	
			100	**100**			
			⇑✓	⇑✓			
1	Existing	—	79	75	87	79	85
	Modified	Mean	—	88 ↑	86 ∘	**87**	**100** ⇑
	Modified	FLP	—	86 ↑	86 ∘	⇑✓	✓
	Modified	Mean-	—	86 ↑	**92**	**87**	**100**
	Modified	zm	—	—	⇑✓	⇑✓	⇑✓
	Modified	FLP-zm	—	86↑	**92**	**87**	**100**
		Trend			⇑✓	⇑✓	⇑✓
					92	**88**	98 ⇑
					⇑✓	⇑✓	**100**
						88	⇑✓
						⇑✓	

↑: increased effect. < effect. of the existing related method for some of the time windows; ⇑: increased effect. ≥ effect. of the existing related method for all different time windows; ∘: (same effect - 3%) ≥ effect. of the existing related method for different time windows; —: decreased effect.; ✓: selected modified method; Bolded: best selected modified methods over each of the methods separately.

- Tests 1 to 5: all time window sizes (half, one, two, three and five cycles),
- Tests 6 to 9: (half, one, two, and three cycles),
- Test 10: (half, one and two cycles).
- Tests 11 to 15: (half, one, two, and three cycles),

Hence, there are 15 test cases for testing the methods during half, one, and two cycle windows, 14 tests for three cycle windows, and 5 tests for five cycle windows. Tables 11 gives the number of correct results for existing methods. The methods using half and one-cycle time windows show a good effectiveness which is also improved by selected modified methods, as shown in Table 12.

6. Discussion and future work

6.1. A recommendation of the proposed methods for real-time applications

As an overall conclusion, according to the results of selected modified methods obtained from simulations and field measurements, the fastest and most accurate methods (effectiveness ≥ 95%) for the transient period of sags are:

For fault cases: SM-DPE (PB) (all modifiers, half cycle), SM-RCC (PB)

Table 8
Field-testing cases.

Test no.	Event source	Monitor (kV)	Sampling freq. (kHz)	Vsag. (pu)	Sag duration (s)
1	DS LG-a	20	5	0.22	0.3
2	DS LG-a	20	10	0.34	0.22
3	DS LL-bc	20	10	0.9	0.16
4	DS LLL	20	10	0.9	0.15
5	DS LG-a	400	1	0.65	0.3
6	US LG-c	220	1	0.35	0.06
7	US LLL	110	1	0.07	0.07
8	US LL-ac	110	6.4	0.82	0.06
9	DS LL-ab+LLL	20	6.4	0.02	0.04+0.03
10	DS TE	20	1.6	0.8	0.04
11	DS LG-a	20	1	0.1	0.08
12	DS LL-ac	20	1	0.47	0.08
13	US LG-a	20	1	0.05	0.08
14	US LG-c	20	1	0.07	0.08
15	US LG-c	20	1	0.06	0.08

10–15: measurements are from the directional over current relays installed in a loop topology; 11, 13, 15: substation transformer is grounded by 80-ohm resistance; 14: substation transformer is grounded by Petersen coil.

Table 6
Time windows presenting the largest effectiveness of selected modified methods.

Case	SM-DPE		SM-RCC		SM-DR		SM-CBM		SM-PCSC	
	PB	IB	PB	IB	PB	IB	PB	IB	PB	IB
Fault	0.5	0.5	0.5, 1	0.5	0.5, 1	0.5, 1	0.5, 1	0.5, 1	0.5, 1	0.5, 1
TE	0.5	0.5*	0.5	0.5*	0.5	0.5*	0.5, 1	0.5*	0.5, 1	0.5*

SM: selected modified; *: high effectiveness by existing methods in the half-cycle time window.

Table 7
A comparison of best analytical selected modified methods with machine learning-based methods in the literature [40].

Method	Analytical			Machine learning-based [40]					
Method type	Best SM proposed	Existing employed related to column 1	Existing used related to column 1	SVM with Polynomial kernel			Ensemble on the DT learners by TotalBoost aggregating method		
Sag period	Transient	Transient	Steady-state	Steady-state		Transient	Steady-state		Transient
Used features/ rules	One/two PB modified features	One/two PB features	One/two PB features	34 features	Five opti. features	—	34 features	Five opti. features	—
Acc. of fault cases (%)	SM-RCC[1]–100 (1 cycle)	E-RCC-97 (1 cycle)	E-RCC-95[4]	96.28	98.6%	—	99.11	99.2	—
Acc. of TE cases (%)	SM-DPE[2]–100 (0.5 cycle) SM-RCC[2]–100 (0.5 cycle) SM-PCSC[3]–100 (1 cycle)	E-DPE-87 (0.5 cycle) E-RCC-94 (0.5 cycle) E-PCSC-85 (1 cycle)	E-DPE-85[4] E-RCC-85[4] E-PCSC-87[4]	—	—	—	—	—	—

[1]:all modifiers (1 cycle); [2]: Mean, Mean-zm, Trend modifiers (0.5 cycle); [3]: all modifiers – {FLP-zm} (1 cycle); [4]: Here 3 cycles window is considered as a steady-state window; DT: decision tree.

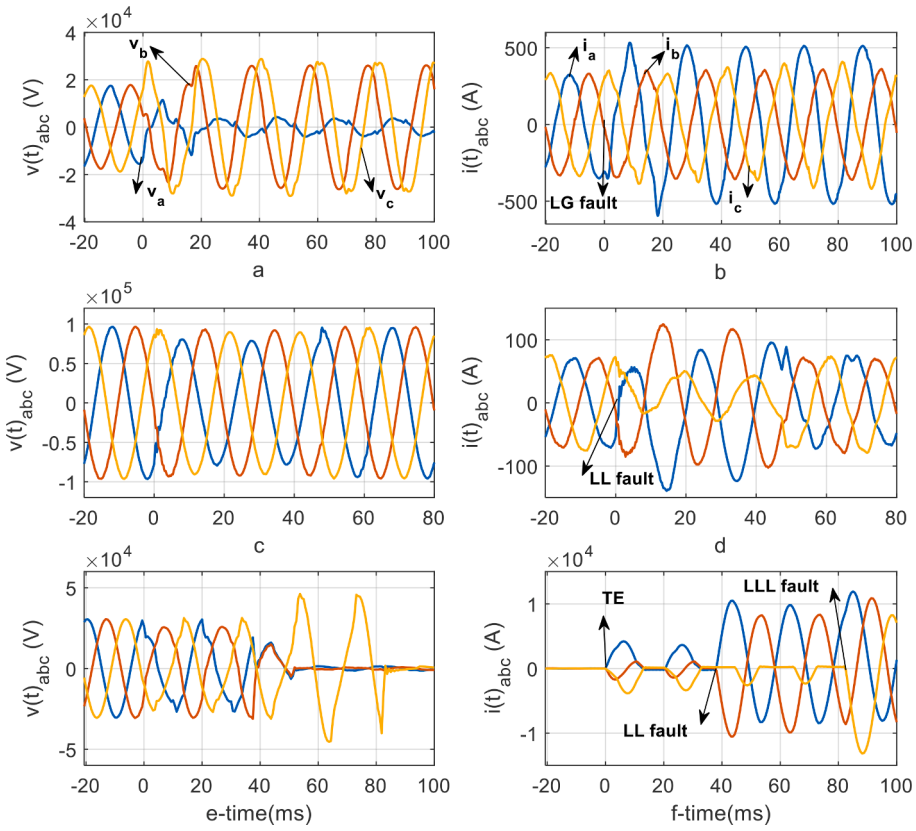

Fig. 16. Line voltages and currents for field testing (a), (b) Test 1, a sag of 0.22 pu due to DS LG-a fault; (c), (d) Test 8, a sag of 0.82 pu due to US LL-ac fault (e), (f) Test 10, a sag of 0.8 pu due to a DS TE followed by LL and LLL faults.

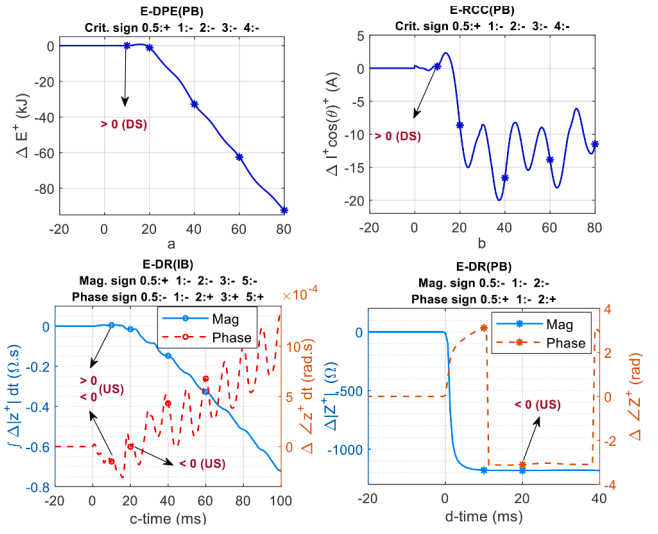

Fig. 17. Field measurement results of existing methods (a), (b) E-DPE (PB) and E-RCC (PB) for US test 8; (c) E-DR (IB) for DS test 1; (d) E-DR (PB) for DS test 10.

(all modifiers, half and one cycle), SM-RCC (IB) (all modifiers-{Trend}, half cycle), and SM-DR (PB) (Trend, one cycle). According to Section 3, a recommendation of the selected modified methods, as good candidates, in order to be used for real-time applications are as follows:

1- SM-DPE (PB) (Mean-zm, FLP-zm, Trend (all 98%), half cycle)
2- SM-RCC (PB) (Mean-zm (99.3%), FLP-zm (99.7%), Trend (99.5%), half cycle)
3- SM-RCC (PB) (Mean-zm, FLP-zm, Trend (all 100%), one cycle)
4- SM-RCC (IB) (Mean-zm (96%), FLP-zm (95%), half cycle)
5- SM-DR (PB) (Trend (96%), 1 cycle)

For TE cases: SM-DPE (PB/IB) (all modifiers, half cycle), SM-RCC (PB/IB) (all modifiers, half cycle), SM-DR, CBM and PCSC (IB) (all modifiers, half cycle), SM-PCSC (PB) (FLP, FLP-zm, Trend, half cycle), and SM-PCSC (PB) (all modifiers, one cycle). According to Section 3, a recommendation of the methods, as good candidates for real-time applications are as follows:

1- SM-DPE (PB) (Mean-zm (100%), FLP-zm (99%), Trend (100%), half cycle)
2- SM-DPE (IB) (Mean-zm, FLP-zm, Trend (all 96.4%), half cycle)
3- SM-RCC (PB) (Mean-zm (100%), FLP-zm (99%), Trend (100%), half cycle)
4- SM-RCC (IB) (Mean-zm, FLP-zm, Trend (all 95.2%), half cycle)
5- SM-PCSC (PB) (FLP-zm, Trend (both 99%), half cycle)
6- SM-PCSC (PB) (Mean-zm (100%), FLP-zm (98%), Trend (100%), one cycle)
7- SM-DR(CBM/PCSC) (IB) (Mean-zm, FLP-zm, Trend (all 100%), half cycle)

Therefore, regardless of the sag sources (either fault or TE), the SM-DPE (PB) (all modifiers, half-cycle), SM-RCC (PB) (all modifiers, half cycle), and SM-RCC (IB) (all modifiers-{Trend}, half cycle) are the best methods. A final recommendation regarding Section 3, regardless of the sag sources, for real-time applications is:

1- SM-DPE (PB) (Mean-zm, FLP-zm, Trend, half-cycle)
2- SM-RCC (PB) (Mean-zm, FLP-zm, Trend, half cycle)
3- SM-RCC (IB) (Mean-zm, FLP-zm, half cycle)

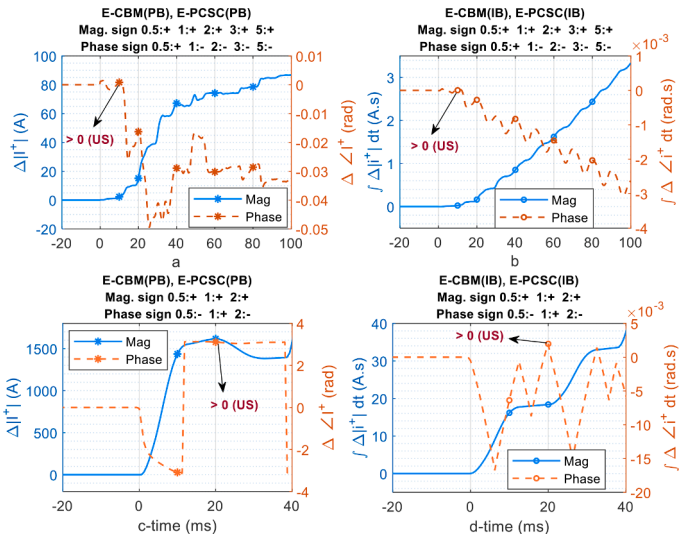

Fig. 18. Field measurement results of existing methods (a) E-CBM (PB) and E-PCSC (PB) for DS test 1; (b) E-CBM (IB) and E-PCSC (IB) for DS test 1; (c) E-CBM (PB) and E-PCSC (PB) for DS test 10; (d) E-CBM (IB) and E-PCSC (IB) for DS test 10.

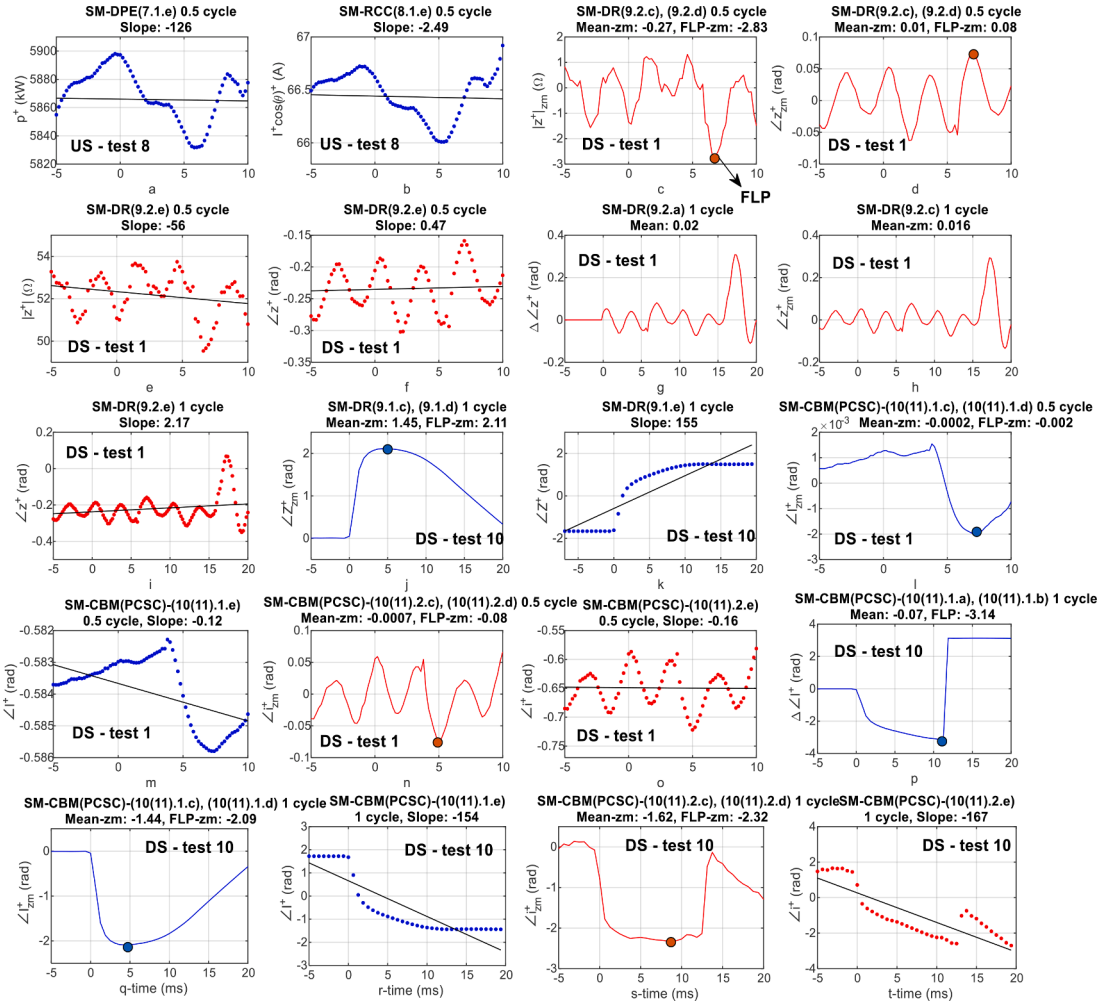

Fig. 19. Time responses obtained by selected modified methods for the field tests shown by arrows in Figs. (17), and (18) during 0.5 or 1 cycle windows. Test number, FLP values, and actual directions are shown inside the figures. Blue and red colors are related to PB and IB methods.

6.2. Future work

The positive-sequence components have been a good solution for the methods, since they exist in any type of fault or other sources of the sags. Because the focus of our study has been on the transmission networks, for which the generation is based mainly on synchronous generators, the

Table 9
Field testing results for a half-cycle time window.

Test no.	E-DPE		SM-DPE		E-RCC		SM-RCC		E-DR		SM-DR		E-CBM		SM-CBM		E-PCSC		SM-PCSC	
	PB	IB	PB	IB	PB	IB	PB	IB	PB	IB	PB	IB	PB	IB	PB	IB	PB	IB	PB	IB
1	✓	✓	✓	✓	✓	✓	✓	✓	✓	×[e]	✓	✓[f]	×[g]	×[h]	✓[i]	✓[j]	×[f]	×[g]	✓[i]	✓[j]
2	✓	✓	✓	✓	✓	✓	✓	✓	×	×	×	×	×	×	×	×	×	×	×	×
3	✓	✓	✓	✓	✓	✓	✓	✓	✓	✓	✓	✓	✓	✓	✓	✓	✓	✓	✓	✓
4	✓	✓	✓	✓	✓	✓	✓	✓	✓	✓	✓	✓	✓	✓	✓	✓	✓	✓	✓	✓
5	✓	×	✓	×	✓	✓	✓	✓	✓	✓	✓	✓	✓	✓	✓	✓	✓	✓	✓	✓
6	✓	✓	✓	✓	✓	✓	✓	✓	✓	✓	✓	✓	✓	✓	✓	✓	✓	✓	✓	✓
7	✓	✓	✓	✓	✓	✓	✓	✓	✓	✓	✓	✓	✓	✓	✓	✓	✓	✓	✓	✓
8	×[a]	✓	✓[b]	✓	×[c]	✓	✓[d]	✓	✓	✓	✓	✓	✓	✓	✓	✓	✓	✓	✓	✓
9	✓	✓	✓	✓	✓	✓	✓	✓	×	✓	×	✓	×	✓	×	✓	×	✓	×	✓
10	✓	✓	✓	✓	✓	✓	✓	✓	✓	✓	✓	✓	✓	✓	✓	✓	✓	✓	✓	✓
11	✓	✓	✓	✓	✓	✓	✓	✓	×	×	✓	×	✓	✓	✓	✓	✓	✓	✓	✓
12	✓	✓	✓	✓	✓	✓	✓	✓	✓	✓	✓	✓	×	×	✓	✓	×	×	×	×
13	✓	✓	✓	✓	✓	✓	✓	✓	✓	×	✓	✓	✓	✓	✓	✓	✓	✓	✓	✓
14	✓	✓	✓	✓	✓	✓	✓	✓	✓	✓	✓	✓	✓	×	✓	×	✓	×	✓	×
15	✓	✓	✓	✓	✓	✓	✓	✓	✓	✓	✓	✓	✓	✓	✓	✓	✓	✓	✓	✓

×: incorrect; ✓: correct; ✓: improvement by SM method; [a]: example shown in Fig. 17a; [b]: Fig. 19a (correct by only (7.1.e)); [c]: Fig. 17b; [d]: Fig. 19b (correct by only (8.1.e)); [e]: Figs. 17c; [f]: Fig. 19c, d, e, and f; [g]: Fig. 18a; [h]: Fig. 18b; [i]: Figs. 19l and m; [j]: Figs. 19n and o.

Table 10
Field testing results for a one-cycle time window.

Test no.	E-RCC	SM-RCC	E-DR		SM-DR		E-CBM		SM-CBM		E-PCSC		SM-PCSC	
	PB	PB	PB	IB	PB	IB	PB	IB	PB	IB	PB	IB	PB	IB
1	✓	✓	✓	×[a]	✓	✓[b]	✓	✓	✓	✓	✓	✓	✓	✓
2	✓	✓	×	×	×	×	×	×	×	×	×	×	×	×
3	✓	✓	✓	✓	✓	✓	✓	✓	✓	✓	✓	✓	✓	✓
4	✓	✓	✓	✓	✓	✓	✓	✓	✓	✓	✓	✓	✓	✓
5	✓	✓	✓	✓	✓	✓	✓	✓	✓	✓	✓	✓	✓	✓
6	✓	✓	✓	✓	✓	✓	✓	✓	✓	✓	✓	✓	✓	✓
7	✓	✓	✓	✓	✓	✓	✓	✓	✓	✓	✓	✓	✓	✓
8	✓	✓	✓	✓	✓	✓	✓	✓	✓	✓	✓	✓	✓	✓
9	✓	✓	×	✓	×	✓	×	✓	×	✓	×	✓	×	✓
10	✓	✓	×[c]	✓	✓[d]	✓	×[e]	×[f]	✓[g]	✓[h]	×[e]	×[f]	✓[g]	✓[h]
11	✓	✓	×	×	×	×	✓	✓	✓	✓	✓	✓	✓	✓
12	✓	✓	✓	✓	✓	✓	✓	✓	✓	✓	✓	✓	✓	✓
13	✓	✓	✓	×	✓	✓	✓	✓	✓	✓	✓	✓	✓	✓
14	✓	✓	✓	✓	✓	✓	✓	×	✓	×	✓	×	✓	×
15	✓	✓	✓	✓	✓	✓	✓	✓	✓	✓	✓	✓	✓	✓

E: existing method; SM: Selected modified methods; ×: incorrect; ✓: correct; ✓: improvement by SM method; [a]: example shown in Fig. 17c; [b]: Figs. 19 g, h and i; [c]: Fig. 17d; [d]: Figs. 19j and k; [e]: Fig. 18c; [f]: Fig. 18d; [g]: Figs. 19p and q; [h]: Figs. 19 s and t.

Table 11
Number of correct results of existing methods for different cycle time windows related to field tests.

Time window (cycle)	E-DPE		E-RCC		E-DR		E-CBM		E-PCSC	
	PB	IB	PB	IB	PB	IB	PB	IB	PB	IB
0.5	14/15	14/15	14/15	15/15	12/15	11/15	11/15	11/15	11/15	11/15
1	15/15	14/15	15/15	15/15	11/15	11/15	12/15	12/15	12/15	12/15
2	15/15	14/15	14/15	15/15	12/15	12/15	11/15	12/15	11/15	12/15
3	13/14	13/14	13/14	14/14	12/14	11/14	11/14	11/14	11/14	11/14
5	5/5	4/5	5/5	5/5	4/5	4/5	4/5	4/5	4/5	4/5

Table 12
Number of correct results of selected modified methods for different cycle time windows for field tests.

Time window (cycle)	SM-DPE		SM-RCC		SM-DR		SM-CBM		SM-PCSC	
	PB	IB	PB	IB	PB	IB	PB	IB	PB	IB
0.5	15/15	14/15	15/15	15/15	13/15	13/15	13/15	13/15	12/15	12/15
1	– – –	– – –	15/15	– – –	12/15	13/15	13/15	13/15	13/15	13/15

—: not existing selected modified method according to Table 4.

positive sequences were employed in the PB and IB methods, both existing and proposed, although the impact of the negative sequence was investigated for asymmetrical sags [11]. In the active distribution networks with the presence of multiple inverter-based distributed generations, the different voltage support control strategies [53,54] may affect the methods during both transient and steady-state periods. Using

the characteristics for only positive sequences and the current limiting mode of inverters was already investigated [22,23] on the PB methods during the steady-state periods. Other voltage support strategies, like using both characteristics for positive and negative sequences of voltages and currents and their impact on the existing and proposed PB and IB methods, can be future work. The different control strategies may also change the transient periods of sags.

Another future work is the real-time implementation of the recommended methods in the previous Section in a software and hardware package. amongst them, the SM-DPE (7.1.c), SM-DPE (7.1.d), SM-RCC (8.1.c), SM-RCC(8.1.d), SM-RCC (8.2.c), and SM-RCC(8.2.d), within a half-cycle period, do not need another algorithm to detect the sag starting time. Also, the SM-DPE (7.1.e) and SM-RCC (8.1.e) are not sensitive to the exact detection of the sag starting time.

7. Conclusion

This paper has investigated the positive-sequence phasor-based and instantaneous-based methods for detecting the location of voltage sag sources within both transient and steady-state periods. Moreover, to reach a more accurate and faster response, new methods were proposed using transient signals obtained from half and one-cycle time windows of sags. These new methods were based on five different proposed modifiers applied in the transient period of voltage sags. Mean and FLP on the signal changes due to sag, Mean, and FLP on a zero-mean signal, and a Trend of the criteria's trajectories versus time around the sag were the proposed modifiers. Evaluating the existing and new methods on extensive numerical simulations showed that the results reveal that the proposed modifiers, used in the new methods, improved ineffective methods, and kept the increased accuracy (due to applying them within a transient period of sags) of other existing methods. A selection was made amongst the new methods in order to choose the most accurate time window (half or one cycle) for each of the methods, and the performances on field measurements showed faster and more effective responses during a transient period of sags.

Regardless of the sag sources, the fastest and most accurate methods (effectiveness $\geq$ 95%) for the transient period were obtained as: SM-DPE (PB) (all modifiers, half-cycle), SM-RCC (PB) (all modifiers, half cycle), and SM-RCC (IB) (all modifiers-{Trend}, half cycle). The recommended methods, along with a voltage sag/fault inception time detection algorithm, can be used for real-time applications.

Using either new methods or a set of rules extracted from a transient period of sags, input to machine learning tools in a supervised backup protection framework reduces the probability of unwanted operation of protection. Moreover, the new methods can be used in directional overcurrent protection of medium voltage networks.

Declaration of Competing Interest

The authors declare that they have no known competing financial interests or personal relationships that could have appeared to influence the work reported in this paper.

Acknowledgments

The authors acknowledge Prof. Math H.J. Bollen, Head of the Power-Engineering Group at the LTU, Skelleftea campus, for his support during this research.

Author statement

All authors certify that they have participated sufficiently in the work to take public responsibility for the content, including participation in the concept, design, analysis, writing, or revision of the manuscript. Furthermore, each author certifies that this material or similar material has not been and will not be submitted to or published in any other publication before its appearance in the EPSR.

References

[1] M. Bollen, I. Gu, Signal Processing of Power-Quality Disturbances, Wiley-IEEE Press, 2006.
[2] M. Bollen, Understanding Power Quality Problems: Voltage Sags & Interruptions, IEEE Press, 2000.
[3] Y. Mohammadi, et al., Locating source of voltage sags: full review, introduction of generalized methods and numerical simulations, Renew. Sustain. Energy Rev. 77 (2017) 821–844.
[4] Marcos V. Costa, et al., A novel methodology for determining the voltage sag impact factor, Electric Power Syst. Res. 174 (2019), 105865.
[5] A.C. Parsons, et al., A direction finder for power quality disturbances based upon disturbance power and energy, IEEE Trans. Power Delivery 15 (3) (July 2000) 1081–1086.
[6] R.C. Leborgne, R. Makaliki, Voltage sag source location at grid interconnections: a case study in the Zambian system, in: 2007 IEEE Lausanne Power Tech, Lausanne, 2007, pp. 1852–1857.
[7] F.O. Passos, et al., An alternative approach to locating voltage sag source side at the point of common coupling based on power-flow information, J. Control, Autom. Electrical Syst. 26 (5) (2015) 579–587.
[8] N. Hamzah, et al., A New approach to locate the voltage sag source using real current component, Electric Power Systems Res. 72 (2) (2004) 113–123.
[9] C. Li, et al., Method for voltage sag-source detection by investigating slope of the system trajectory, in: IEE Proceedings - Generation, Transmission and Distribution 150, 2003, pp. 367–372.
[10] T. Tayjasanant, et al., A resistance sign-based method for voltage sag source detection, IEEE Trans. Power Delivery 20 (4) (Oct. 2005) 2544–2551.
[11] W. Kanokbannakorn, T. Saengsuwan, S. Sirisukprasert, Unbalanced voltage sag source location identification based on superimposed quantities and negative sequence, in: The 8th Electrical Engineering/Electronics, Computer, Telecommunications and Information Technology (ECTI) Association of Thailand, Khon Kaen, 2011, pp. 617–620.
[12] A.K. Pradhan, A. Routray, Applying distance relay for voltage sag source detection, IEEE Trans. Power Delivery 20 (1) (2005) 529–531.
[13] S. Zhenguo, P. JinPing, K. Jian, Locating voltage sag source with impedance measurement, in: 2010 International Conference on Power System Technology, Hangzhou, 2010, pp. 1–6.
[14] C. Liu, et al., A Method of voltage sag source location considering source load characteristics, in: 12th International Conference on Intelligent Computation Technology and Automation (ICICTA), 2019, pp. 566–569.
[15] Y. Yilin, X. Yonghai, Research of method for voltage sag source detection in power distribution network, in: 2011 6th IEEE Conference on Industrial Electronics and Applications, Beijing, 2011, pp. 485–488.
[16] R.C. Leborgne, D Karlsson, Voltage sag source location based on voltage measurements only, Electric Power Qual. Utilization 14 (1) (2008) 25–30.
[17] J. Blanco, J.F. Petit, G. Ordóñez, Algorithm for relative location of voltage sags and capacitor switching transients based on voltage measurements only, in: 16th International Conference on Harmonics and Quality of Power (ICHQP), 2014, pp. 833–837.
[18] M.H. Moradi, Y. Mohammadi, A new current-based method for voltage sag source location using directional overcurrent relay information, Int. Trans. Electrical Energy Systems 23 (2) (Mar. 2013) 270–281.
[19] M.H. Moradi, Y. Mohammadi, M. Hosseini-Tayyebi, A novel method to locate the voltage sag source: a case study in the Brazilian power network (Mato Grosso), Przegląd Elektrotechniczny (Electrical. Review) 88 (33b) (2013) 112–115.
[20] A.K. Pradhan, et al., Fault direction estimation in radial distribution system using phase change in sequence current, IEEE Trans. Power Delivery 22 (4) (Oct. 2007) 2065–2071.
[21] M.H. Moradi, Y. Mohammadi, Voltage sag source location: a review with introduction of a new method, Int. J. Electr. Power Energy Syst. 43 (1) (Dec. 2012) 29–39.
[22] Y. Mohammadi, R.C Leborgne, Improved DR and CBM methods for finding relative location of voltage sag source at the PCC of distributed energy resources, Int. J. Electr. Power Energy Syst. 117 (2020) 1–18.
[23] Y. Mohammadi, R.C Leborgne, A new approach for voltage sag source relative location in active distribution systems with the presence of inverter-based distributed generations, Electric Power Syst. Res. 189 (2020).
[24] S.J. Ahn, et al., A new approach to determine the direction and cause of voltage sag, J. Electrical Eng. Technol. 3 (3) (2008) 300–307.
[25] V. Barrera, et al., Voltage sag source location from extracted rules using subgroup discovery, Artif. Intell. Res. Develop. 148 (2008) 225–235.
[26] V.B. Nunez, et al., Evaluation of fault relative location algorithms using voltage sag data collected at 25-kV substations, Int. Trans. Electrical Energy Syst. 20 (2010) 34–51.
[27] B. Polajžer, et al., Evaluation of different methods for voltage sag source detection based on positive-sequence components, Renew. Energy Power Qual. J. 1 (07) (2009) 150–154.
[28] B. Polajžer, et al., Detection of voltage sag sources based on instantaneous voltage and current vectors and orthogonal clarke's transformation, IET Gener. Trans. Distrib. 2 (2) (2008) 219–226.
[29] B. Polajžer, et al., Generalization of methods for voltage sag source detection using vector-space approach, IEEE Trans Ind Appl 45 (6) (2009) 2152–2161.

[30] B. Polajžer, et al., Detection of voltage sag sources based on the angle and norm changes in the instantaneous current vector written in clarke's components, Int. J. Electr. Power Energy Syst. 64 (2015) 967–976.
[31] B. Polajžer, et al., Instantaneous positive-sequence current applied for detecting voltage sag sources, IET Gener. Trans. Distrib. 9 (4) (2015) 319–327.
[32] Y. Mohammadi, et al., Employing instantaneous positive-sequence symmetrical components for voltage sag source relative location, Electric Power Syst. Res. 151 (Oct. 2017) 186–196.
[33] B. Solak, T Sikorski, Analysis of voltage dip source location methods, Modern Electric Power Syst. (MEPS) (2019) 1–6.
[34] Y. Mohammadi, R.C. Leborgne, Relative location of voltage sags source at the point of common coupling of constant power loads in distribution systems, Int. Trans. Electrical Energy Syst. (2021) e12516.
[35] Wei Kong, et al., Voltage sag source location based on instantaneous energy detection, Electric Power Systems Res. 78 (11) (2008) 1889–1898.
[36] A.W. Ling, H. Shareef, A single monitor method for voltage sag source location using Hilbert-Huang Transform, Res. J. Appl. Sci. Eng. Technol. 5 (1) (2013) 192–202.
[37] C. Xiaodong, et al., Research on location and recognition method of voltage sag disturbance, IOP Conf. Ser. (2020).
[38] H. Shareef, A. Mohammad, A.A Ahmed, Identification of voltage sag source location using S and TT transformed disturbance power, J. Central South University 20 (2013) 83–97.
[39] Y. Mohammadi, et al., A novel method for voltage-sag source location using a robust machine learning approach, Electric Power Syst. Res. 145 (2017) 122–136.
[40] Y. Mohammadi, et al., Comprehensive strategy for classification of voltage sags source location using optimal feature selection applied to support vector machine and ensemble techniques, Int. J. Electr. Power Energy Syst. 124 (2021) 1–21.
[41] K. Ding, et al., Convolutional neural network for voltage sag source azimuth recognition in electrical internet of things, Wireless Commun. Mobile Comput. 2021 (2021) 11, pages.
[42] L. Chaozhang, et al., Voltage sag source location based on comprehensive criterion and neural network method, IOP Conf. Ser.: Earth Environ. Sci. 512 (2020), 012131.
[43] Y. Deng, et al., Sag source location and type recognition via attention-based independently recurrent neural network, J. Modern Power Syst. Clean Energy (2021) in press.
[44] W. Lizhen, Z. Yongnian, H. Xiaohong, C. Wei, Research on a location method for complex voltage sag sources based on random matrix theory, Math. Probl. Eng. 2020 (2020) 12, pages.
[45] J.C. Filho, et al., Optimized Method for Locating the Source of Voltage Sags, J. Commun. Softw. Syst. 17 (2) (2021) 197–202.
[46] R.A. Oliveira, et al., Comparative analysis of transformer-energizing and fault-caused voltage dips on the dynamic behaviour of DFIG-based wind turbines, IEEE PES Innov. Smart Grid Technol. Europe (2020) 589–593.
[47] C.O. Henao, et al., Towards active distribution networks fault location: contributions considering DER analytical models and local measurements, Int. J. Electr. Power Energy Syst. 99 (2018) 454–464.
[48] F.V. Lopes, et al., Real-time traveling-wave-based fault location using two-terminal unsynchronized data, IEEE Trans. Power Delivery 30 (3) (2015) 1067–1076.
[49] Dian. Lu, Yu. Liu, D. Lu, B. Wang, X. Zheng, Unsynchronized fault location on untransposed transmission lines with fully distributed parameter model considering line parameter uncertainties, Electric Power Syst. Res. 202 (1) (2022), 107622.
[50] F. Kleber de Araújo Lima, J.M. Guerrero, F.L. Tofoli, C.G.C. Branco, Dantas JL. Fast and accurate voltage sag detection algorithm, Int. J. Electr. Power Energy Syst. 135 (2022).
[51] B. Polajžer, S. Gorazd, S. Sebastián, D. Drago, Impact of asymmetrical disturbance events on voltage sag source detection, Renew. Energy Power Qual. J. 1 (2007).
[52] L.A.D. Costa, Y. Mohammadi, R.C. Leborgne, D.D.S. Gazzana, Impact evaluation of the neutral-grounding resistance on short-duration RMS voltage variations, in: 19th International Conference on Harmonics and Quality of Power, 2020, pp. 1–6.
[53] M.E. Meral, D. Çelík, A comprehensive survey on control strategies of distributed generation power systems under normal and abnormal conditions, Ann. Rev. Control 47 (2019) 112–132.
[54] D. Çelik, M.E. Meral, Voltage support control strategy of grid connected inverter system under unbalanced grid faults to meet fault ride through requirements, IET Gener. Trans. Distrib. 14 (2020) 3198–3210.